https://doi.org/10.1016/j.ccr.2017.10.015

This is the Pre-Published Version.

Coord. Chem. Rev. (Special Issue on "Coordination Chemistry for Energy")

Molecular/polymeric metallaynes and related molecules: solar cell materials and devices

Linli Xu*[a], Cheuk-Lam Ho*[a,b], Li Liu*[c], Wai-Yeung Wong*[a,b]

[a] *Department of Applied Biology and Chemical Technology, The Hong Kong Polytechnic University, Hung Hom, Hong Kong, P. R. China*

[b] *Department of Chemistry, Hong Kong Baptist University, Waterloo Road, Hong Kong, P. R. China*

[c] *Hubei Collaborative Innovation Center for Advanced Organic Chemical Materials, Ministry of Education Key Laboratory for the Synthesis and Application of Organic Functional Molecules, School of Chemistry and Chemical Engineering, Hubei University, Wuhan 430062, P. R. China*

Received XXXXX

Corresponding authors.

E-mail address: linli.xu@polyu.edu.hk (L. Xu), cheuk-lam.ho@polyu.edu.hk (C.-L. Ho), liulihubei@hubu.edu.cn (L. Liu), wai-yeung.wong@polyu.edu.hk (W.-Y. Wong).

© 2017. This manuscript version is made available under the CC-BY-NC-ND 4.0 license https://creativecommons.org/licenses/by-nc-nd/4.0/

Abstract

Energy remains one of the great challenges for the world. There is a considerable interest in developing renewable energy resources and improving the technologies for energy conversion. In this context, solar energy is a source with the proven capacity to meet the increasing global energy needs. In recent years, efficient organic solar cells (OSCs) have been fabricated using organic polymers and small molecules. Metalated conjugated organic molecules have also been shown to be good alternatives to the all-organic congeners and have demonstrated good promise as solar cell materials in OSCs and dye-sensitized solar cells (DSSCs). Among these, soluble molecular/polymeric metallaynes and their acetylide-functionalized metalloporphyrins show promising results in much of these investigations with the best power conversion efficiencies of 9.06% (for single-layer OSC), 12.5% (for tandem OSC) and 13.2% (for co-sensitized DSSC) to date. This review summarizes the recent advances of this field. Various factors influencing the device performance such as the nature of metal center and organic spacer, absorption coefficient, bandgap energy, charge carrier mobility, accessibility of triplet excitons and blend film morphology of these materials will be discussed. Given the diversity of transition metals available (for example, Pt, Zn, Ru) and structural versatility of the organic

components, it is anticipated that this nascent field using metalated organic materials would continue to lead to exciting prospects in the near future.

Keywords: acetylide; dye-sensitized solar cell; metallayne; organic solar cell; transition metal

Contents

Abbreviations: A, electron acceptor; BHJ, bulk heterojunction; bpy, 2,2'-bipyridine; BTD, benzothiadiazole; C_{60}, buckminsterfullerene; D, electron donor; DFT, density functional theory; DIO, 1,8-diiodooctane; D−A, donor-acceptor; DFT, density functional theory; DPP, diketopyrrolopyrrole; DSSC, dye-sensitized solar cell; E_A, LUMO energy level of the acceptor; E_D, HOMO energy level of the donor; E_g, optical bandgap; EQE, external quantum efficiency; FF, fill factor; HOMO, highest occupied molecular orbital; ICT, intramolecular charge transfer; IPCE, incident photon-to-electron conversion efficiency; LUMO, lowest unoccupied molecular orbital; NIR, near infrared; OSC, organic solar cell; P_{out}, power output; P_{in}, power input; PCE, power conversion efficiency; $PC_{61}BM$ (or $PC_{71}BM$), [6,6]-phenyl-C_{61} (or C_{71})-butyric acid methyl ester; PET, photoinduced electron transfer; P3HT, poly(3-hexylthiophene); PSC, polymer solar cell; SCLC, space-charge limited current; TCNE, tetracyanoethylene; TCNQ, 7,7,8,8-tetracyanoquinodimethane; TD-DFT, time-dependent density functional theory; η_A, absorption efficiency; η_{ED}, efficiency of exciton diffusion; η_{CT}, efficiency of charge transfer; η_{CC}, charge collection efficiency; J_{sc}, short-circuit current density; V_{oc}, open-circuit voltage; μ_h, hole mobility; ε, absorption coefficient.

1. Introduction

Human survival and civilization considerably depend on low-cost and sustainable energy. Human demand for energy is ever increasing, being driven by growing population, rising economies and improving the standard of living in many parts of the world [1−3]. The International Energy Agency projects a 48% increase in global energy consumption from 2012 to 2040 [1]. At present, fossil fuels contribute to 80% of the global energy consumption and will continue to be the major player in the global energy landscape [1, 3]. So, a major global issue nowadays is the upcoming depletion of fossil fuels in the foreseeable future and the energy crisis. While our quality of life depends significantly on the availability of energy, one of the current grand challenges is to develop innovative materials that would provide new sources of clean sustainable energy or to develop processes that can lead to efficient utilization of energy. Renewable energy sources such as solar, wind and hydroelectric power can provide massive amounts of energy to solve most of our immediate energy needs and fight for a more sustainable environment [4]. The current global annual energy consumption was approximately 13 TW from which fossil fuels still account for most of the energy supply. This would, however, translate into huge annual emissions of greenhouse gas CO_2, causing many detrimental environmental problems. By 2050, global energy demand is projected to increase to about 30 TW, which requires at least

an extra 17 TW in the next 33 years when our fossil fuel reserves are varnishing [5].

Sunlight is the most abundant source of energy on Earth and a promising solution to our energy crisis because the Earth receives more energy from the Sun in an hour than is necessary for all humanity within a year. While photovoltaic production presents the world's fastest-growing energy technology, much research has gone into producing efficient solar (photovoltaic) cells [6]. Although silicon and inorganic semiconductors (e.g. crystalline and amorphous Si and recently, CdTe and $CuInGaSe_2$ thin films) have still dominated the production market and remain frontline precursors in the fabrication of solar cells, their performance and competitiveness are now challenged by emerging polymer solar cells (PSCs) [7−11]. The low cost, flexibility, light weight and easy processability of polymers allow the fabrication of cost-competitive plastic solar cells for specialty and commodity applications. Organic solar cell materials are also chemically versatile and can be synthesized in large quantities under moderate conditions. Therefore, conjugated organic polymers are becoming eminent candidates for PSCs which can be fabricated by solution-processing technologies and scaled up for production of large-area and mechanically-flexible devices [12].

Due to the rapid recent progress in PSCs, impressive power conversion efficiencies (PCEs) over 10% have been accomplished for PSCs based on both single-

junction and tandem architectures, revealing their great potential toward practical applications and commercialization. Although organic polymers are still dominating the PSC field, a novel approach which has not been largely explored to capture sunlight for electricity generation involves putting metal elements into conjugated organic polymer backbones. It is well-known that metalated compounds have become prevalent in DSSCs in which the Grätzel-type solar cell owes much success to this area [13]. Hence, complementary to the pure organic molecules, metal-containing conjugated polymers represent another versatile class of molecular and polymeric semiconductors for OSCs. The installation of transition metals into conjugated polymer scaffolds offers many advantages and the presence of transition metal elements may endow the polymer with the following attributes [14]: (i) the redox centers can mediate charge transfer and enhance the electronic properties, (ii) the heavy metal centers can facilitate intersystem crossing from the lowest singlet (S_1) to triplet (T_1) excited states, and the efficiency of charge generation can be increased by harnessing the triplet excited states in these photovoltaic materials, in which the triplet excitons also have longer lifetimes and thus allow extended exciton diffusion lengths, (iii) the metal ions may act as architectural templates to control the self-assembly of the organic subunits via various metal-metal and/or metal-ligand interactions, (iv) metal ions allow fine-tuning of the gap between the highest occupied molecular

orbital (HOMO) and lowest unoccupied molecular orbital (LUMO) through the interaction of the metal d-orbitals with the ligand orbitals that can control charge transport, (v) metal orbitals can donate or accept a charge to or from ligand orbitals, forming charge transfer complexes with unique optoelectronic properties, and (vi) there is a diversity of molecular framework based on different coordination number, geometry and valence shell of different metal atom. These attributes would make metal-based organic donor or photosensitizing molecules a promising class of compounds for OSCs and DSSCs.

This review is devoted to providing an in-depth survey and a better understanding of the solar cell materials and devices based on the molecular and polymeric metallaynes which also include the recent cutting-edge works on acetylide-functionalized metalloporphyrin donor materials. Here, we will also pay particular attention on the utility of alkyne bonds that can affect the optoelectronic and structural properties as well as the overall device performance.

2. Organic solar cells

2.1. Device structure

In a bulk heterojunction (BHJ) PSC, the photoactive layer is sandwiched between a transparent anode and a low-work-function metal cathode (Fig. 1). Typical

BHJ PSCs consist of mixed electron-donating conjugated polymers and electron-accepting fullerene (or non-fullerene) derivatives as the photoactive layer, which can effectively absorb sunlight and generate excitons that can dissociate in the interfacial layer to produce the photocurrent. This configuration allows efficient separation of photogenerated excitons into free charges and provides a favorable charge transport route at the donor-acceptor (D−A) interface to the electrodes. BHJs made from bicontinuous polymer-fullerene composites are currently the main configurations for highly efficient PSCs which can be configured in two forms (Fig. 2) [13]. In inorganic semiconductors, the binding energy is usually small as compared to the thermal energy at room temperature, which favors generation of photoinduced free charges under ambient conditions. However, the higher exciton binding energy of an organic semiconductor typically produces excitons instead of free charges upon photoexcitation [15]. In PSC, it requires a mechanism to dissociate the excitons [15], and D−A interface is necessary to maximize the interfacial area between the two components and dissociate bound electron-hole pairs to generate free charges [13].

Buckminsterfullerene (C_{60}) and its soluble derivatives, [6,6]-phenyl-C_{61} (or C_{71})-butyric acid methyl ester (PCBM or $PC_{71}BM$), are promising electron acceptor materials known for OSCs/PSCs [7−11]. The state-of-the-art PSCs are represented by BHJs based on a phase-separated blend of PCBM and poly(3-hexylthiophene)

(P3HT), with reproducible PCE approaching 5% [16]. To date, much effort has been devoted to developing new organic donor materials, and establishing what their properties they should have to afford efficient solar cells by blending the donors with fullerene or non-fullerene acceptors.

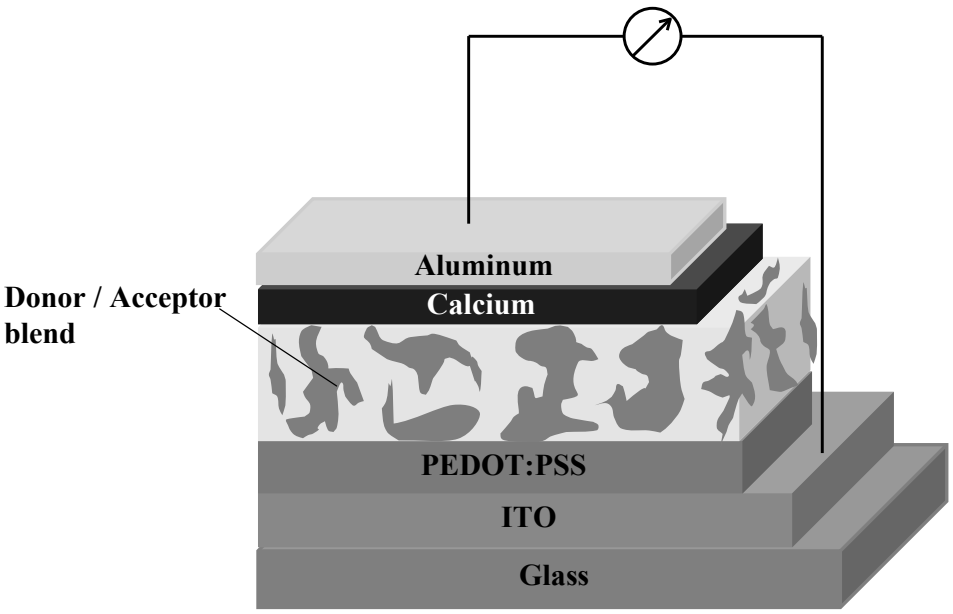

Fig. 1. A typical structure of a BHJ solar cell.

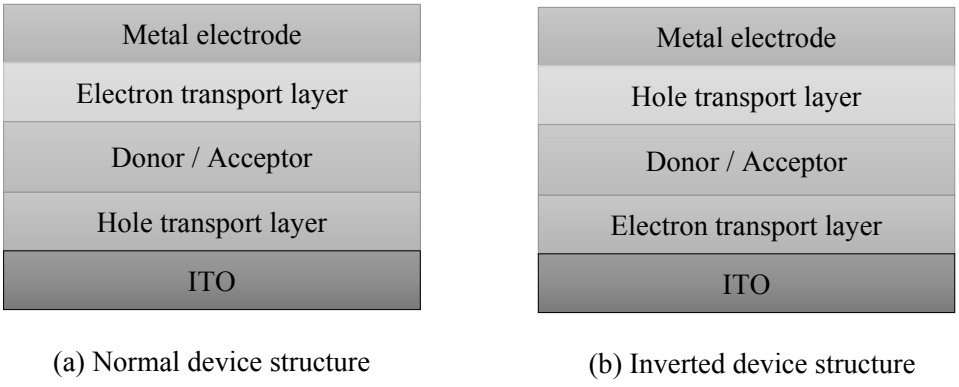

Fig. 2. Two different BHJ device structures.

2.2. The working mechanism

An understanding of how a BHJ cell functions is critical in developing a strategy to improve its performance. Typically, a BHJ cell operates in four main steps: (i) absorption of an incident light photon and generation of an exciton, (ii) diffusion of the exciton toward a D–A interface, (iii) photoinduced separation of the exciton into free charges at the D–A interface, and (iv) collection of charges at the electrodes (Fig. 3) [17]. The donor material has a smaller HOMO (with respect to the vacuum level) and LUMO as compared with the acceptor, As such, the donor is the hole transporting material and ideally makes ohmic contact with the anode, whereas the acceptor material transports electrons and contacts the cathode. In the first step, the absorption efficiency (η_A) is largely determined by the absorption spectra of the organic layers and their thickness, as well as by the device architecture. The efficiency of exciton diffusion process (η_{ED}) is controlled mainly by the exciton diffusion length and the morphology of the D-A interface. The exciton dissociation process for the creation of free charges is characterized by an efficiency (η_{CT}) that is significant if energetically favorable. The final step, which is governed by the charge collection efficiency (η_{CC}), represents the percentage of dissociated excitons that are collected at the electrodes and is mainly sensitive to the morphology and mobility of the active layers. Any of these steps can be modulated to tune the efficiency of the cell, but exciton diffusion

lengths and charge separation affect PCE more than the others [18]. A strategy is to increase the exciton diffusion length, and facilitate charge separation to reduce charge recombination. As a triplet excited charge transfer state with a long lifetime increases the exciton diffusion length, and eventually promotes charge separation [19−22], it is likely that the formation of a triplet excited state would enhance the efficiency. It is established that heavy atoms, such as transition metals, allow singlet–triplet intersystem crossing via spin-orbit coupling to enable the formation of the triplet excited charge transfer state [14, 18, 19−22]. Thus, the integration of transition metal complexes within BHJ cells should favor formation of a triplet excited state and a triplet exciton favorably undergoes charge separation as recombination is spin–forbidden and the long lifetimes of triplet excited states ensure that the exciton reaches the D–A interface [21]. Indeed, results validate the enhanced performance of polymer BHJ solar cells when a transition metal-containing polymer is used as an electron donor (vide infra) [23].

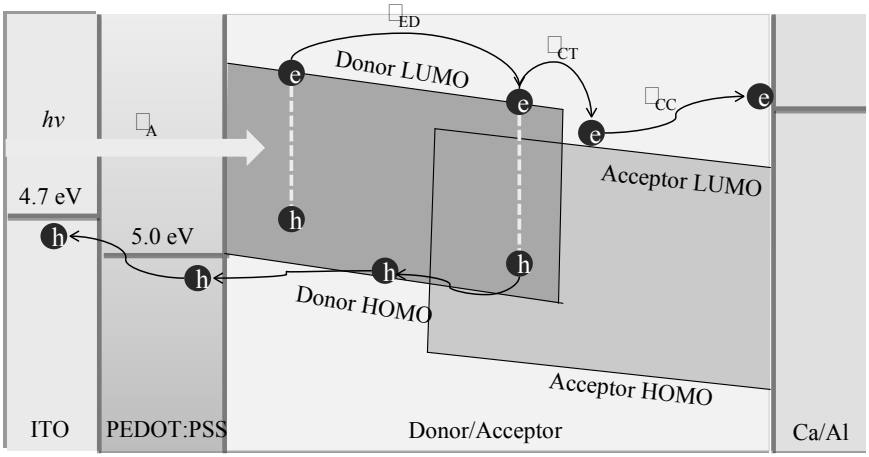

Fig. 3. Main processes in a BHJ solar cell.

4.1. Device performance indicators

Generally, PSC device performance expressed in terms of PCE depends on the light-harvesting capability of the photoactive layer, the charge carrier mobility of both electron-donating and electron-accepting materials, charge separation and the extraction efficiency. Different processing methods can result in differences in BHJ morphology and consequently different device performance. Optimization of the processing procedure is usually dependent upon the solvent evaporation kinetics, viscosity effects and shear stresses during solvent evaporation [24]. Fig. 4 depicts the typical current density (J)−voltage (V) characteristics of a BHJ device under light illumination. The solar cell efficiency depends on a number of interrelated factors to get the best values of open-circuit voltage (V_{oc}), short-circuit current density (J_{sc}) and fill factor (FF) (Fig. 4). The PCE is defined as power output (P_{out}) divided by power input (P_{in}), and is typically governed by the product of the V_{oc}, J_{sc} and FF (see equations (1) and (2)).

$$\mathrm{PCE} = \frac{P_{\mathrm{out}}}{P_{\mathrm{in}}} = \frac{P_{\mathrm{max}}}{P_{\mathrm{in}}} = \frac{V_{\mathrm{max}} \times J_{\mathrm{max}}}{P_{\mathrm{in}}} = \frac{V_{\mathrm{oc}} \times J_{\mathrm{sc}} \times \mathrm{FF}}{P_{\mathrm{in}}} \quad (1)$$

$$\mathrm{FF} = \frac{V_{\mathrm{max}} \times J_{\mathrm{max}}}{V_{\mathrm{oc}} \times J_{\mathrm{sc}}} \quad (2)$$

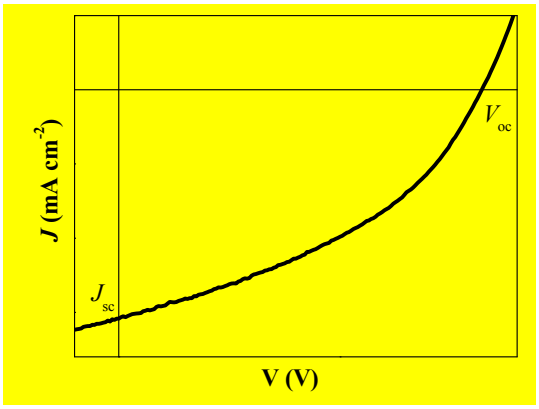

Fig. 4. A typical *J*-*V* characteristic curve of a BHJ solar cell.

Fig. 5 shows a schematic drawing of the energy levels in a BHJ cell. The V_{oc} of a BHJ device is proportional to the difference between the HOMO energy level of the donor material E_D and the LUMO energy level of the acceptor E_A, according to equation (3)

$$V_{oc} = 1/e[E_D - E_A] - 0.3 \quad (3)$$

where e is the elementary charge and the value of −4.3 eV is used for the LUMO energy level of PCBM. The value of 0.3 V is an empirical factor [25].

A theoretical estimation predicts that 10% efficiency can be achieved for single-layer cells from a polymer donor with a HOMO–LUMO gap of 1.74 eV [26]. A downhill LUMO energy offset of 0.3 eV between polymer and fullerene is required to trigger the exciton splitting and charge dissociation for an ideal polymer [26]. This is a kinetic issue based on the Marcus reorganization energy. A value less than 0.3 V as the driving force leads to very slow event and therefore the exciton will be wasted. A certain offset of the HOMO and LUMO energy levels (ΔE_{HOMO} and ΔE_{LUMO}) is also

required to overcome the exciton binding energy for exciton dissociation [27].

A polymer donor should also possess a lower HOMO energy level to give a higher V_{oc} value. The J_{sc} is dependent on the light-harvesting properties of the photoactive layer, charge carrier mobility of both electron donor and acceptor, and the charge extraction efficiency. Ideally, the absorption spectra of the polymers should be broad and strong in intensity to match the solar spectrum to achieve high J_{sc} value. The FF depends on the non-geminated charge carrier recombination, the film processing method and hence the film morphology. So, in order to enhance the overall photovoltaic performances of PSCs, it is necessary to improve every photovoltaic parameter, which demands careful optimization of the optical bandgap (E_g) and the corresponding absorption coefficient of both electron donor (D) and electron acceptor (A) materials, the frontier energy levels, film morphology, interfacial engineering and the appropriate use of device architectures.

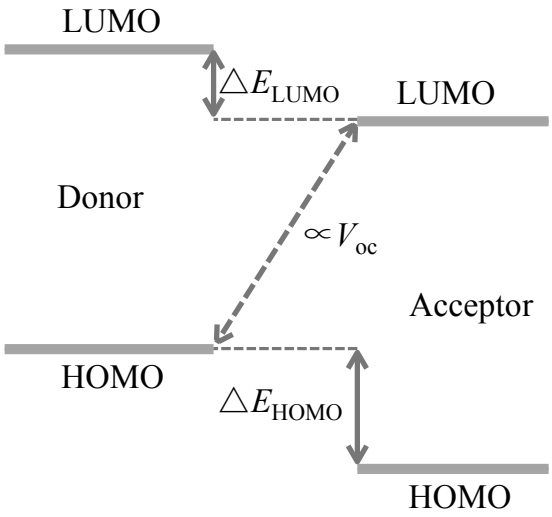

Fig. 5. A schematic drawing of the donor and acceptor energy levels.

5. Molecular and polymeric metallaynes and related solar cell materials

3.1. Polyplatinaynes and their small-molecular congeners

The pioneering work on semiconducting polyacetylene is an important breakthrough in the field of organic optoelectronics. Since then, poly(aryleneethynylene)s represent a useful class of polymers for PSCs [28]. To date, metallopolymers based on Pt(II)-aryleneethynylene building blocks are among the most extensively investigated Pt(II)-containing materials for OSCs (Table 1) [29, 30] and the prototype for such investigation is focused on the Pt(II) polyyne **1**. When Pt ions are conjugated with alkyne units to form a one-dimensional polymer chain, the d-orbitals of the Pt ions overlap with the p-orbitals of the alkyne units, leading to an enhancement of both π-electron delocalization and intrachain charge transport along the polymer chain. This orbital overlap enhances the spin-orbit coupling and facilitates the intersystem crossing from the singlet to triplet manifolds, hence enhancing the formation of triplet excitons which have longer lifetimes and thus allow extended exciton diffusion lengths. The generally good solubility of Pt polyynes over their organic poly(heteroaryleneethynylene)s also favors good film formation and fabrication via solution processing. The charge transport in Pt-acetylides has also been demonstrated in the literature [31, 32].

The first report on the photovoltaic effect was given by Köhler et al. in 1994 for

a wide bandgap polymer **1** [33]. The maximum photocurrent quantum yields for carrier generation in single-layer neat polymer cells of ITO/**1**/Al were ~0.03−0.6%, and the performance was comparable to that found in similar devices made with poly(phenylenevinylene). Using a platinum-containing π-conjugated polymer **1** as a donor material and C_{60} as an acceptor, Köhler et al. also observed efficient charge separation and transfer [34]. Photoluminescence studies reveal that the addition of 7 wt% of C_{60} to the polymer **1** quenches phosphorescence more than fluorescence. Also, the phosphorescence lifetime decreases after addition of C_{60}, indicating that triplet excited state is involved in the charge transfer process. Although the binding energy of the triplet exciton is high (~0.8 eV), the long lifetime (2.1 μs) associated with the triplet excited state ensures favorable charge transfer to the C_{60} acceptor [34]. The photovoltaic cell of ITO/**1**:C_{60}/Al generates current at a quantum yield of 1−2% [34].

Afterwards, the Pt polyynes with oligothiophenes as the spacer were prepared and the E_g value follows the order of **4** < **3** < **2**, in line with an enhanced π-electron delocalization along the series. The photocells with configuration of Au/**2**/Al, ITO/**3**/Al and ITO/**4**/Al were fabricated, which resulted in the maximum photocurrent quantum yield of ~0.04% at the first photocurrent peak, V_{oc} of 0.47−0.75 V and FF of 0.30–0.35 [35]. For **2**-based cell, it was shown that the photocurrent was increased by enhancing exciton dissociation in the polymer film but decreased after annealing

under vacuum [36]. Schanze et al. also demonstrated the beneficial role of transition metals in BHJ solar cells [19−22]. For polymer **2**, it was shown that platinum-induced formation of the triplet excited state facilitates photoinduced charge transfer to enhance the PCE of solar cells [19−22]. The authors observed the quenching of phosphorescence from the polymer, and unequivocally proved the existence of the triplet excited state of the polymer, the absence of an energy transfer quenching pathway, and the presence of electron transfer to a fullerene acceptor [21]. The photovoltaic cell fabricated with **2** as the donor material afforded an impressive IPCE of 0.16–0.27%, depending on the thickness of the photoactive layer **2**:PCBM (1:4 wt%) (see Table 1) [21].

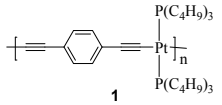

1

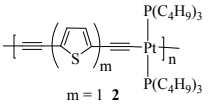

m = 1 **2**
m = 2 **3**
m = 3 **4**

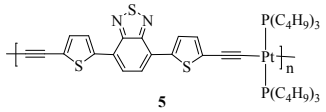

5

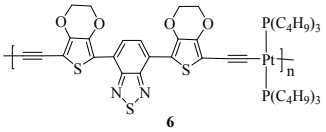

6

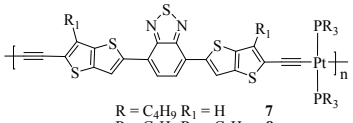

R = C_4H_9 R_1 = H **7**
R = C_4H_9 R_1 = C_8H_{17} **8**
R = Et R_1 = C_8H_{17} **9**

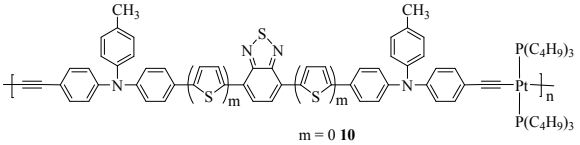

m = 0 **10**
m = 1 **11**

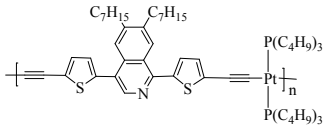

12

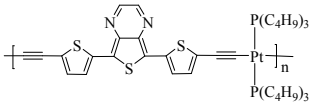

13

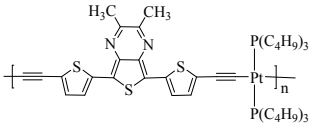

14

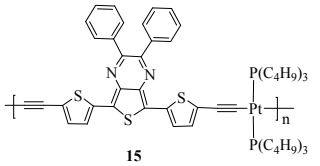

15

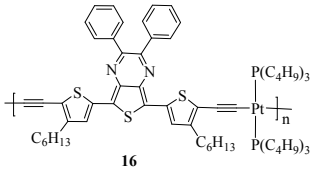

16

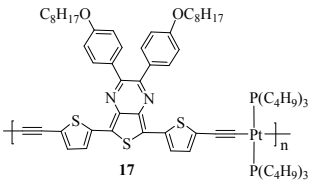

17

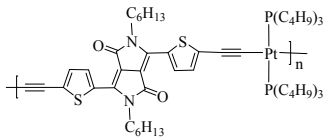

18

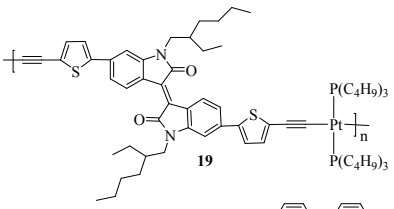

19

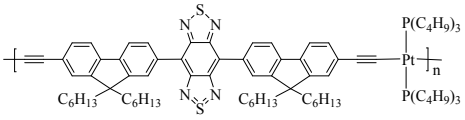

20

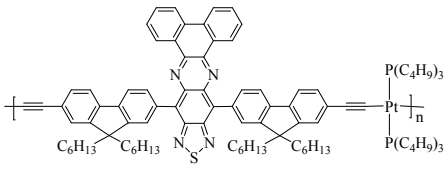

21

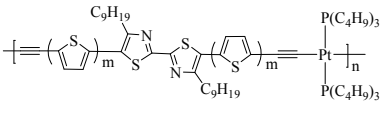

m = 0 **22**
m = 1 **23**
m = 2 **24**
m = 3 **25**

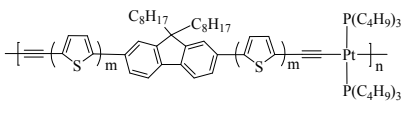

m = 0 **26**
m = 1 **27**
m = 2 **28**
m = 3 **29**

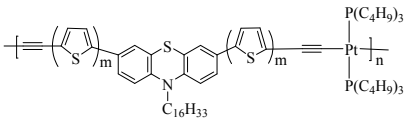

m = 0 **30**
m = 1 **31**
m = 2 **32**

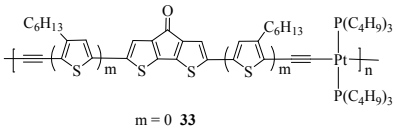

m = 0 **33**
m = 1 **34**

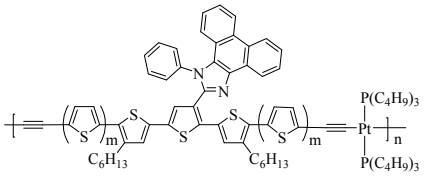

m = 0 **35**
m = 1 **36**

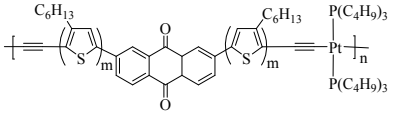

m = 0 **37**
m = 1 **38**

The breakthrough in organometallic photovoltaics came from the work by Wong et al., where the narrow-bandgap D−A polymer **5** with 4,7-di-2'-thienyl-2,1,3-benzothiadiazole as the core component was exploited [37]. This polymer absorbs strongly at 554 nm and its bandgap (E_g = 1.85 eV) is significantly lowered by about 0.35–0.70 eV relative to the purely electron-rich bithienyl (E_g = 2.55 eV) (**3**) or electron-deficient benzothiadiazole (2.20 eV) counterpart [38]. It was shown that charge transfer excited state rather than the triplet state contributes to the efficient photoinduced charge separation for **5**, which is different from **2**-based blends where the triplet state is involved in charge separation. The BHJ solar cells with **5**/PCBM blends delivered an average PCE of 4.1% with V_{oc} of 0.82 V, J_{sc} of 13.1 mA cm^{-2} and FF of 0.37. Using polymer **5** as an example, the effects of the parameters such as blend ratio, choice of casting solvent, thickness of active layer and type of cathode on the PCE have been studied (Fig. 6). The blend ratio is an important parameter in controlling the morphology and phase separation of the film. For **5**:PCBM blend, there is a significant enhancement in PCE when comparing the best efficiency (1:4) to the worst one (1:1) (Fig. 6a). The best blend ratio between donor and acceptor was 1:4 w/w because of a better phase separation. Formation of PCBM-rich domains improved charge transport and carrier collection efficiency, which led to a reduction of recombination losses and an increase in J_{sc}. The solvent effects were examined for

5 (Fig. 6b) and there is a dramatic difference in PCE among different solvent conditions. The influence of casting solvent is likely related to the degree of roughness and topography of the film obtained by spin-coating. The size of the PCBM-rich domains in the blend film changes with the choice of solvent, which affects the phase separation and morphology. The blend film prepared by toluene and chlorobenzene solutions had a slow evaporation time compared to the chloroform solution, and a slower evaporation time results in a rougher film. The different solubility of PCBM in different solvents also interferes with the phase separation of the film. Generally, the optimal thickness of active layer represents a compromise between absorption and charge collection. A thicker layer will absorb more light, but increased thickness will result in a lower charge collection because of the low charge carrier mobilities (Fig. 6c) [39]. By changing the cathode, the V_{oc} had a difference of ~0.15 V between Al and Mg:Ag for **5**:PCBM blend (Fig. 6d), because of the pinning of Fermi level of the electrodes to the reduction potential of PCBM.

By replacing the thiophene ring in **5** with 3,4-ethylenedioxythiophene, a deep-blue metallopolyyne **6** was obtained which showed strong visible light absorption and low E_g [40]. However, the PSC performance was not good (PCE = 0.78%) as compared to that of **5**. Jen and co-workers reported a series of amorphous Pt(II) polymers with rigid thieno[3,2-*b*]thiophene-2,1,3-benzothiodiazole spacer **7–9** which

exhibited field-effect hole mobility up to 1.0×10^{-2} cm^2 $V^{-1}s^{-1}$ [41]. These polymers display absorption maxima within 587–611 nm in the solid state with low E_g (1.81−1.85 eV), which are attributed to the intramolecular charge transfer (ICT) between D and A units. The hole mobility (μ_h) was significantly improved from 1.6×10^{-5} cm^2 $V^{-1}s^{-1}$ in **5** to 1.5×10^{-3} cm^2 $V^{-1}s^{-1}$ in **7**. By adding the alkyl chain on the thieno[3,2-*b*]thiophene moiety in **8** and **9**, μ_h was further improved to 1.0×10^{-2} cm^2 $V^{-1}s^{-1}$. The relatively high μ_h of **8** and **9** may be attributed to the amorphous thin film characteristics due to the steric hindrance between the bulky $Pt(PR_3)_2$ groups. These reveal that the more rigid spacer structure facilitates the electron coupling between D and A units along the polymer backbone and results in the strongly enhanced charge-transporting property of polyplatinaynes. Polymer **8** exhibited a PCE of 3.57% with high V_{oc} of 0.81 V, J_{sc} of 8.67 mA cm^{-2} and FF of 0.51, whereas **9** showed very good PSC performance (PCE = 4.13%, V_{oc} = 0.79, J_{sc} = 10.12 mA cm^{-2}, FF = 0.52) due to its high μ_h. Device made from **9**:$PC_{71}BM$ gave an enhanced PCE as it possessed a large phase separation compared to a relatively smooth surface morphology.

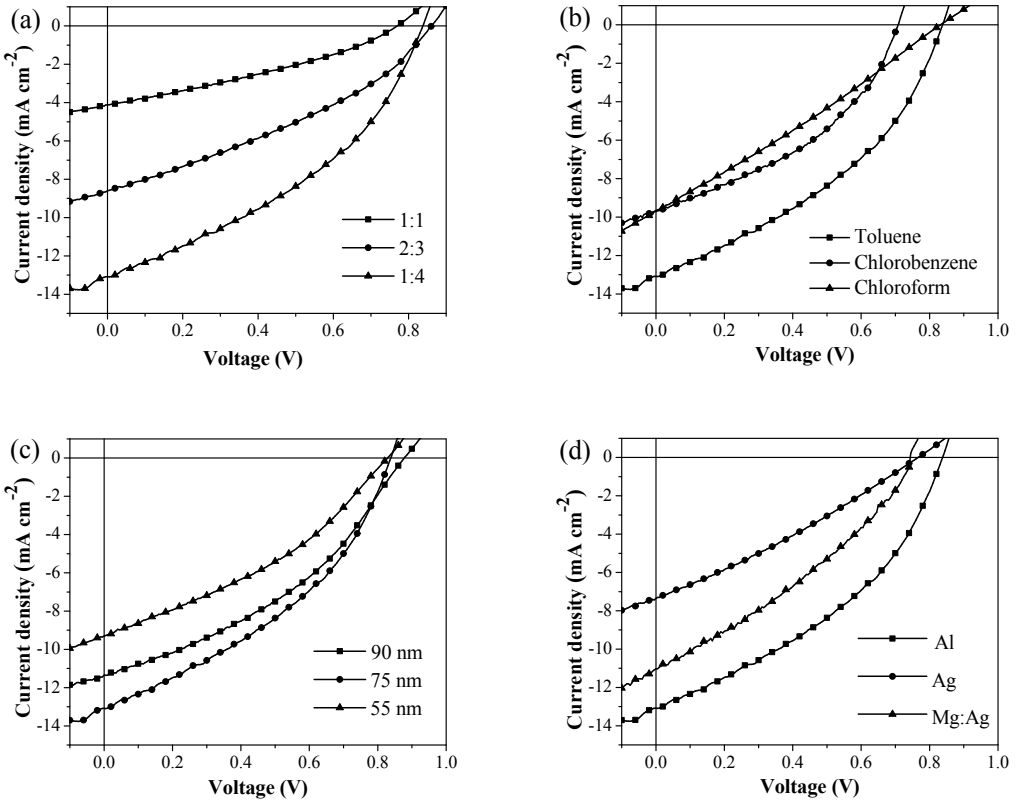

Fig. 6. Effects of different fabrication conditions on the *J*–*V* curves of BHJ solar cells based on **5**/PCBM blend.

The low-bandgap property of **10–11** with D-π-A-π-D structural motif is attributed to the electron-accepting nature of the benzothiadiazole (BTD) unit, which causes significant ICT even in the ground state by coupling with the electron-donating triphenylamino groups [42]. The absorption band of **11** can cover a wide wavelength range within 300–700 nm showing a low HOMO–LUMO gap of 1.85 eV, which is comparable to the E_g value of **5**. The low E_g in **11** favors harvesting of more solar photon energy which results in a PCE of 1.61% with V_{oc} of 0.77 V, J_{sc} of 4.9 mA cm^{-2} and FF of 0.39 in **11**-based device.

By using different strong acceptor units, such as 2,3-diheptylpyrido[3,4-*b*]pyrazine, thieno[3,4-*b*]pyrazine, benzo[1,2-*c*:4,5-*c*']bis([1,2,5]thiadiazole), [1,2,5]thiadiazolo[3,4-*i*]dibenzo[*a*,*c*]phenazine, diketopyrrolopyrrole (DPP) and isoindigo in **12**–**21**, ICT strength of the polymers can be modified with increased absorption coverage in both visible and near infrared (NIR) regions [43−46]. For example, **13**−**17** possess extremely low E_g of 1.47–1.50 eV with broad absorption features in the range of 300–900 nm. Values of J_{sc} = 3.23 mA cm^{-2}, V_{oc} = 0.51 V and PCE = 0.63% were recorded for **16**. Also, **20–21** with specially designed weak donor-strong acceptor electronic traits were used for NIR photovoltaic applications [45]. They possess narrow E_g of 1.54 and 1.65 eV, respectively, and a low HOMO level of about 5.50 eV. The two adjacent relatively weaker fluorene donors instead of thiophene rings are introduced in **20–21** to form D−A−D type of spacers to facilitate the ICT and further reduce the E_g. Since benzo[1,2-*c*:4,5-*c*']bis([1,2,5]thiadiazole) unit is known to possess a substantial quinoidal character, it allows for greater electron delocalization. A red-shift of the long-wavelength peak by 29 nm is observed by increasing the acceptor strength of acceptor unit from **21** to **20**. The bands in the NIR region give rise to strong ICT absorption in **20** and **21**. Solar cell device based on **20** gave rise to a maximum PCE of 1%.

The influences of the number of thienyl rings in the organic spacer on the

absorption, charge transport and solar cell efficiency of Pt(II) polyynes have been examined [14]. In the series of polymers **22**–**38**, increasing the number of oligothienyl rings (m) along the main chain effectively lowers the E_g of the polymers. For example, in the two groups of polymers **22**−**25** and **26**−**29** with m varying from 0 to 3, the E_g of **25** is significantly reduced by ca. 0.34 eV relative to **22**, whereas that of **29** is much reduced by 0.60 eV relative to **26** [47, 48].[50] Their photovoltaic responses and PCE also depend to a large extent on the value of m in the spacer (Fig. 7). Solar cell with peak external quantum efficiency (EQE) of 83% and PCE of up to 2.7% were measured for **24** [47]; while the fluorene-based polyplatinayne **29** gave a PCE of up to 2.9% [48]. Although the E_g of **26–29** are not very low (> 2.3 eV), their high absorption coefficients (ε) and suitable energy levels for interaction with PCBM render them to achieve high efficiency. With a strong blue-absorbing phenothiazine chromophore, high-bandgap polymers **30–32** were prepared (> 2.5 eV), which can be used for photosensitization at a shorter wavelength under solar illumination [49]. The best PCE of 1.3% was attained for **32-**based solar cells. Extremely low E_g of 1.44–1.53 eV falling into the NIR window of the solar spectrum were observed for **33–34** with the electron-deficient 4*H*-cyclopenta[2,1-*b*:3,4-*b*']dithiophen-4-one spacer [51]. By incorporating the D–A side chain tethered phenanthrenyl-imidazole, **35–36** were prepared with E_g from 2.28 to 2.34 eV [51]. By inclusion of the electron-poor

anthraquinone organic moiety, the E_g of **38** was narrowed down to 1.88 eV, and this in turn can raise the performance of the resulting solar cells by 0.33% [52].

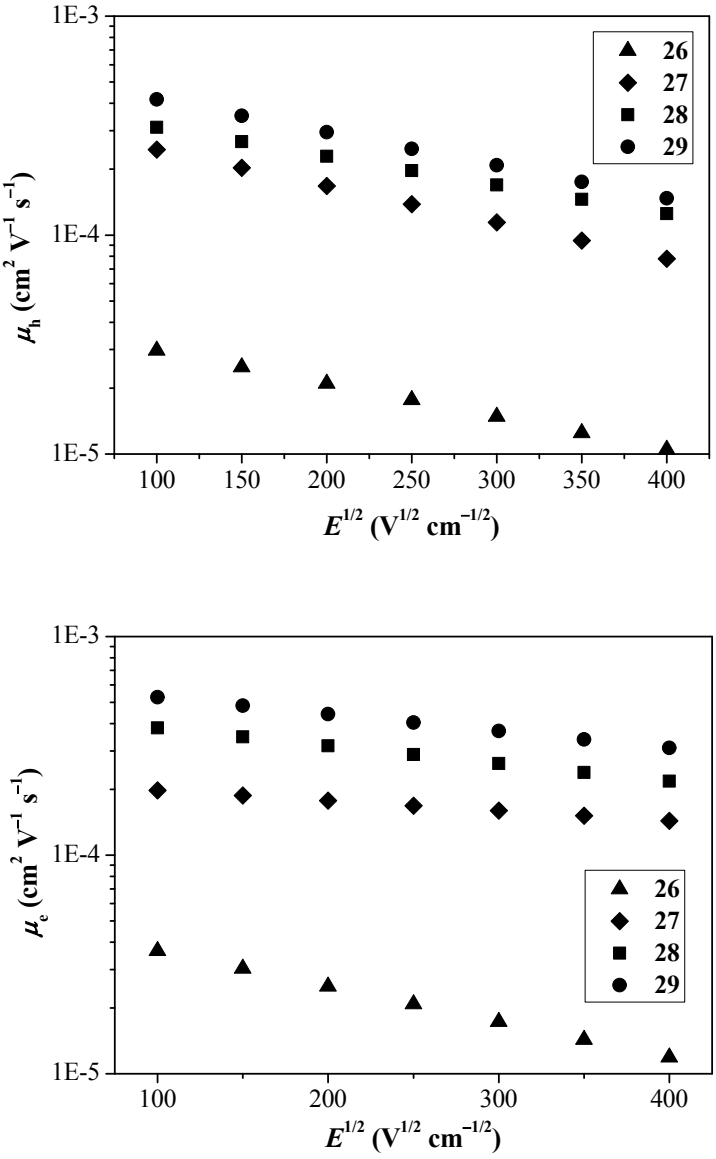

Fig. 7. (a) Hole mobility (μ_h) and (b) electron mobility (μ_e) for **26**−**29**:PCBM blends obtained by the space-charge limited current (SCLC) modeling method.

Polymers with higher dimensionality can be expected to lead to a better photovoltaic performance due to the improved isotropic charge transport and optical

properties. In a proof-of-concept demonstration, Pt(II)-acetylide polymers **39**–**41** with multi-dimensional structures were developed [53]. Higher molecular dimension and longer π-conjugation length induced by fluorene in **41** show more favorable absorption and charge-transport features than that for the linear polymer **39**. Due to the lack of D–A structure in these polymers, **39**–**41** achieved rather high E_g of 2.59–2.72 eV. The ε value of the multi-dimensional polymer **40** is almost double that of **39** (ε = 0.45 × 10^5 cm^{-1} and 1.05 × 10^5 cm^{-1} at 413 nm for **39** and **40**, respectively), and an even higher ε is noted for **41**. The efficiency of BHJ devices based on these polymers increases as the dimensionality increases. The higher PCE of **41** at 2.24% is plausibly attributed to the much improved morphological features and pseudo-three-dimensional charge-transport properties of the active layer.

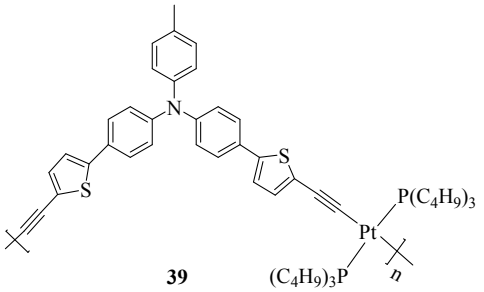

39

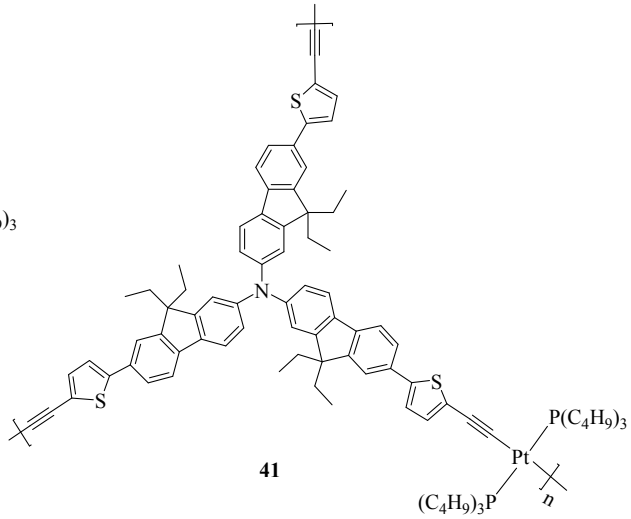

41

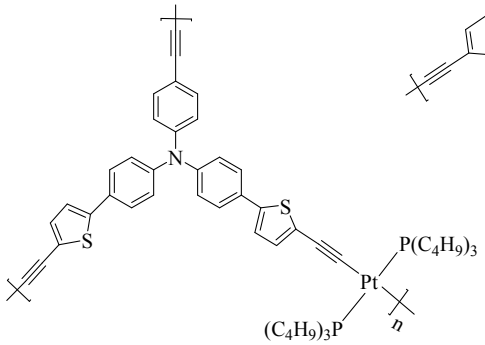

40

Random Pt-containing D−A copolymers with two different electron acceptors

(**42**–**47**) were also prepared and characterized [44]. The absorption spectra of these copolymers are similar in shape with distinct π-π* and ICT absorption bands. Manipulation of E_g and the relative intensity of two ICT bands due to the use of different acceptors was shown by varying the D–A–D pair and the composition of comonomer. While **43** and **44** have very close E_g, both **45** and **46** exhibit similar E_g to that of **13**, suggesting the more dominant contribution of thiophene-thieno[3,4-*b*]pyrazine-thiophene pair. Polymer **45** gives higher absorption intensity at shorter wavelength than **46**. Copolymers containing thieno[3,4-*b*]pyrazine and pyrido[3,4-*b*]pyrazine (**45**−**47**) possess E_g of 1.53−1.55 eV and gave low PCE values (0.09−0.16%). PCE and J_{sc} were shown to increase in the order of **47** < **46** < **45**. However, **45** and **46** exhibited the same V_{oc} (0.5 V) and FF (0.23) while **47** gave a lower FF (0.18). Copolymer **43** afforded the highest PCE of 0.71% among the series. Poor charge separation and charge transport properties of these copolymers led to very low FF values from 0.20 to 0.25.

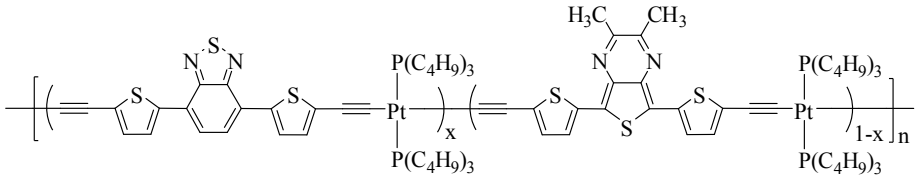

x = 0.50 **42**

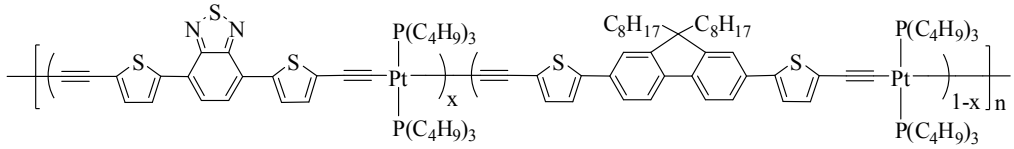

x = 0.50 **43**

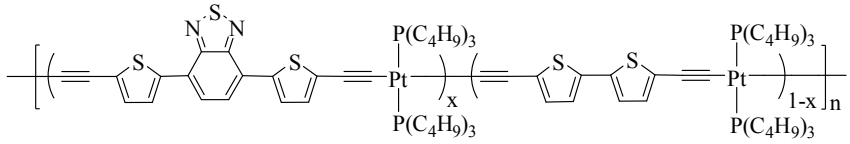

x = 0.50 **44**

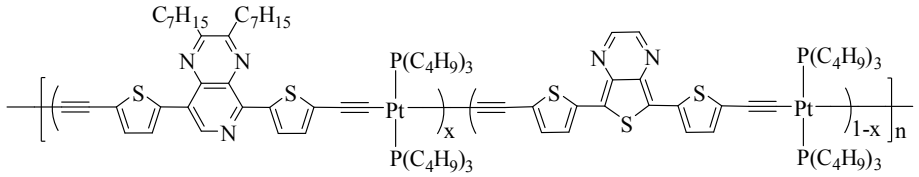

x = 0.50 **45**

x = 0.33 **46**

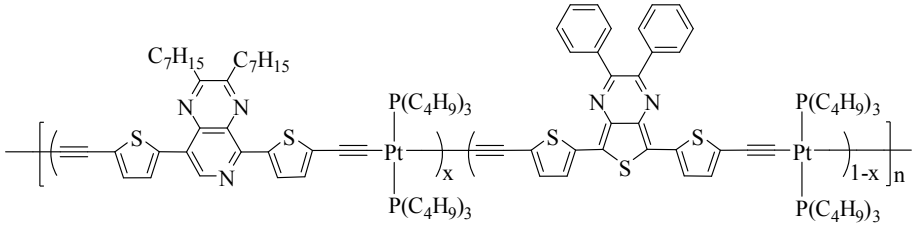

x = 0.29 **47**

Most of the aforementioned Pt-polyyne polymers were used as p-type semiconductors in PSCs. This reveals the intrinsic p-type character of these metal-containing materials. In order to prepare potential n-type materials, post-functionalization method of the Pt-polyyne polymers was employed. It is well-known that metal acetylides are appropriate precursors for the reaction with cyanated acceptors such as tetracyanoethylene (TCNE) and 7,7,8,8-tetracyanoquinodimethane (TCNQ). In particular, the Pt-acetylides have received much attention due to the synthetic versatility as well as the excellent semiconducting character of the

corresponding linear Pt polyyne polymers. Post-functionalization of a Pt(II) polyyne polymer by [2+2]-cycloaddition followed by a cycloreversion of TCNE or TCNQ should result in a significant decrease in E_g in the resulting polymer. Initially, cyanation of polymers **1** and **49a** were carried out by adding TCNE to produce **48** and **49**, respectively, but no detailed analysis was given [54]. Low-bandgap polymers **50** and **51** have also been developed by Michinobu and co-workers using the hexylthiophene unit instead which can enhance the reactivity of acetylene units since thiophene ring is a stronger donor than the phenyl ring [55]. Thanks to the activation of both Pt and thiophene units, the reactions of **50a** with both TCNE and TCNQ can be carried out. As both TCNE and TCNQ units are electron-accepting in nature, both **50** and **51** displayed D–A characteristics as compared to **50a**, which result in broad ICT absorption bands covering the visible to the NIR regions. Polymer **50** possesses a well-defined absorption band at 508 nm and since the TCNQ adduct has a stronger electron-accepting feature than the TCNE one, **51** reveals a more bathochromically shifted wavelength to 598 nm in its absorption spectrum. The E_g of **50** and **51** are 1.83 and 1.22 eV, respectively, which are consistent with a reduction in the D–A interaction between the metal and spacer in **50**. By introducing the electron-accepting BTD and DPP into the main chain, the E_g of **52** and **53** (1.47 and 1.28 eV for **52** and **53**, respectively) notably decrease relative to **50** [56]. Also,

the LUMO levels of the TCNE-adducted polymers **52** and **53** are much lower than those of the precursor polymers. Therefore, functionalization on the triple bonds of polyynes by cyanation is an effective method to lower the E_g and broaden the absorption coverage of the resulting Pt(II) polyyre polymers, which also provides a good way to develop narrow-bandgap n-type polyplatinaynes. While no photovoltaic data were reported for **50** and **51**, Pt-copolymers **52** and **53** were used as the active components of BHJ solar cells. Upon cyanation of the polymers, **52** and **53** showed poorer photovoltaic parameters than those of the devices based on the corresponding precursors without cyano groups. These results reveal the decrease in the p-type performance of the Pt-polyyne polymers by the TCNE addition, which is consistent with the decrease in the energy levels. Attempts were also made to fabricate all-polymer solar cells based on P3HT as the p-type semiconductor and cyanated Pt-polyyne **52** or **53** as the n-type semiconductor. Disappointingly, device made from **52** only gave a PCE of 0.00079% while that from **53** did not even produce any photocurrent [57].

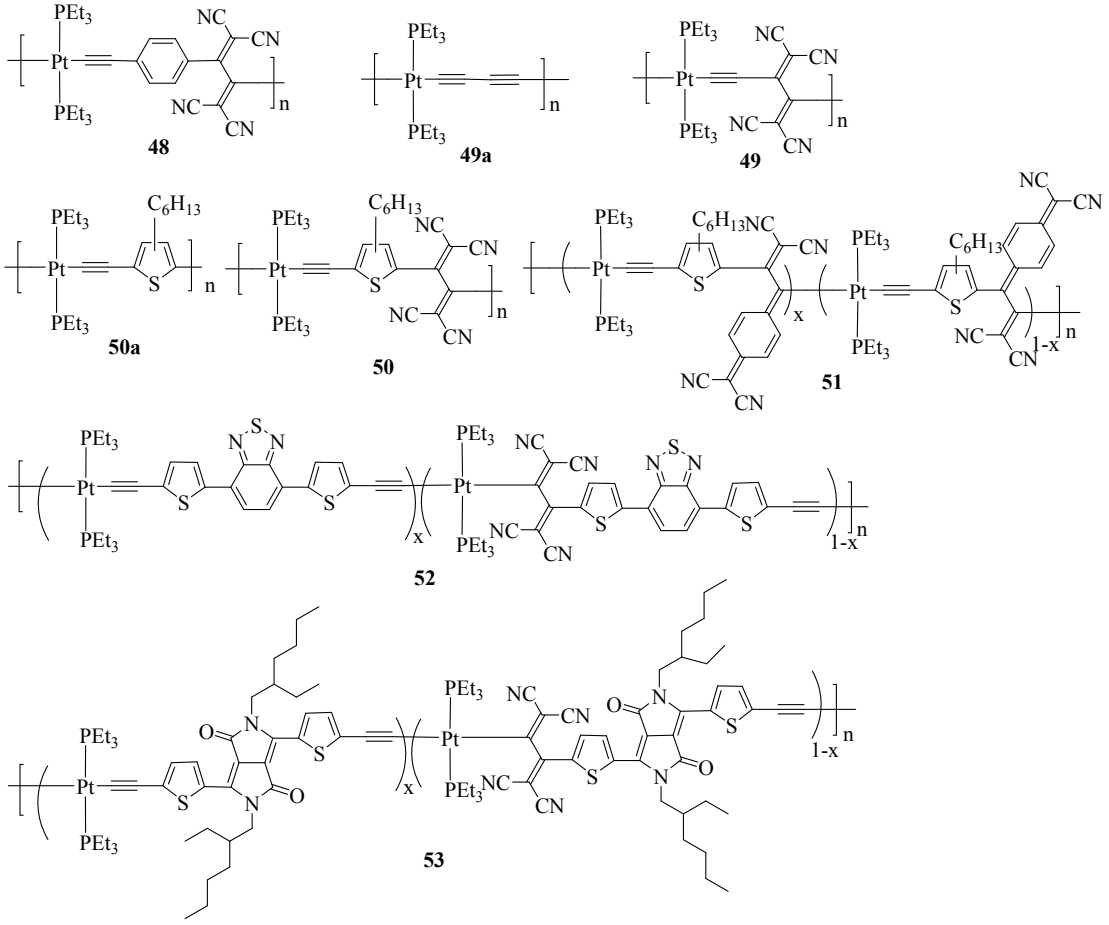

Pt(II) oligoynes **54**−**56** containing BTD as the central core and terminal oligothienyl rings showed the E_g of 1.9 eV and PCE of 2.2−3.0% (Table 2) [58]. The auxiliary ligands PBu_3 on Pt(II) center prevented aggregation of the polymers and offered good solution processability. An increase of the oligothiophene chain length n can red-shift the absorption bands significantly but the effect on the hole mobility is negligible. These oligomers gave V_{oc} of 0.71−0.82 V. Among them, **55** produced the best PCE of 3.0% with J_{sc} of 8.45 mA cm^{-2}. Four metalated conjugated oligothiophenes **57**−**60** with two different accepting end groups were also synthesized and their OSC performance assessed [59]. The low-lying HOMO levels of these

small-sized molecular donors match with the LUMO levels of the PCBM acceptor. The peak PCE at 1.59% was achieved by **58**:$PC_{71}BM$ (3:7), which showed a decline to 1.06% with a change in the blend ratio to 1:4. A similar PCE of 1.56% was also noted by the **60**:$PC_{71}BM$ (1:4) based device. Device made from **57**:PCBM blend gave a PCE of 0.88%, which decreased with increasing the blend ratio. The poor device performance (PCE = 0.17%) was realized for **59**:$PC_{71}BM$ blend with no change in PCE by varying the blend ratio.

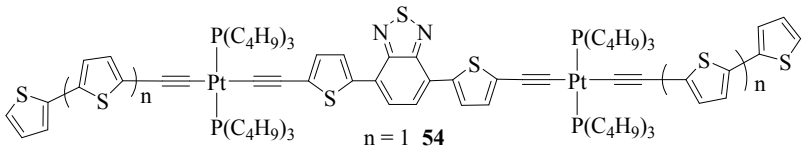

n = 1 **54**
n = 2 **55**
n = 3 **56**

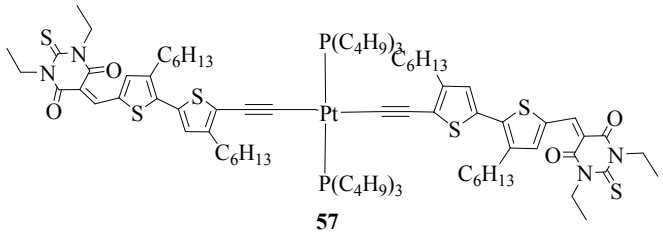

57

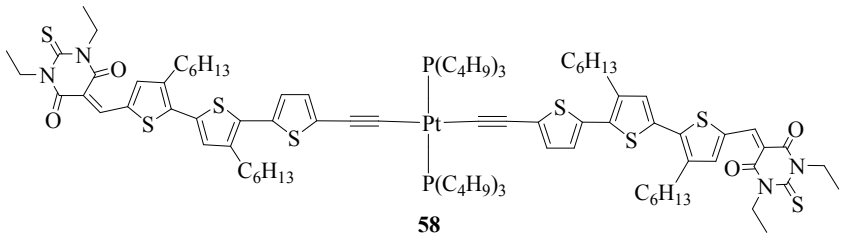

58

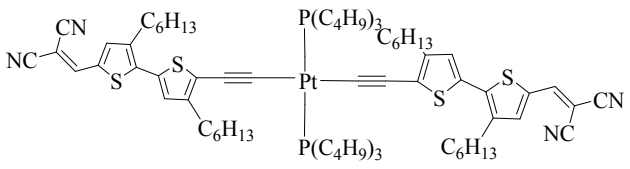

59

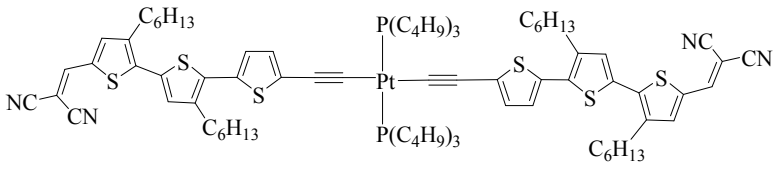

60

Solution-processed Pt(II) σ-bis(aryleneethynylene) complexes also have good potential to excel in developing high-efficiency solar cells without the problem of molecular weight variation commonly observed for the corresponding polymers. Wong et al. have prepared four complexes **61**−**64** in reasonable yields [60]. From the X-ray crystal structures of **64** (Fig. 8), we can see the coplanarity of the di(thienyl)benzothidiazole unit, which helps to improve the absorption. The absorption band can be readily extended into the long-wavelength range above 600 nm by attaching ICT chromophores. As shown from the absorption data, the increase in the electron-donating strength using triphenylamino groups in these complexes caused broadening and enhancement of the ICT transition. This is consistent with the time-dependent density functional theory (TD-DFT) calculations where the HOMOs are mainly delocalized over the aryleneethynylene functionalities and the LUMOs are highly localized on the BTD groups. BHJ solar cells based on **61**:$PC_{71}BM$ (1:4) and **62**:$PC_{71}BM$ (1:4) gave the best photovoltaic performance with PCE values of 2.34−2.37% (IPCE ~45.1−49.3%) in the series which correlate well with the absorption intensity of the ICT band.

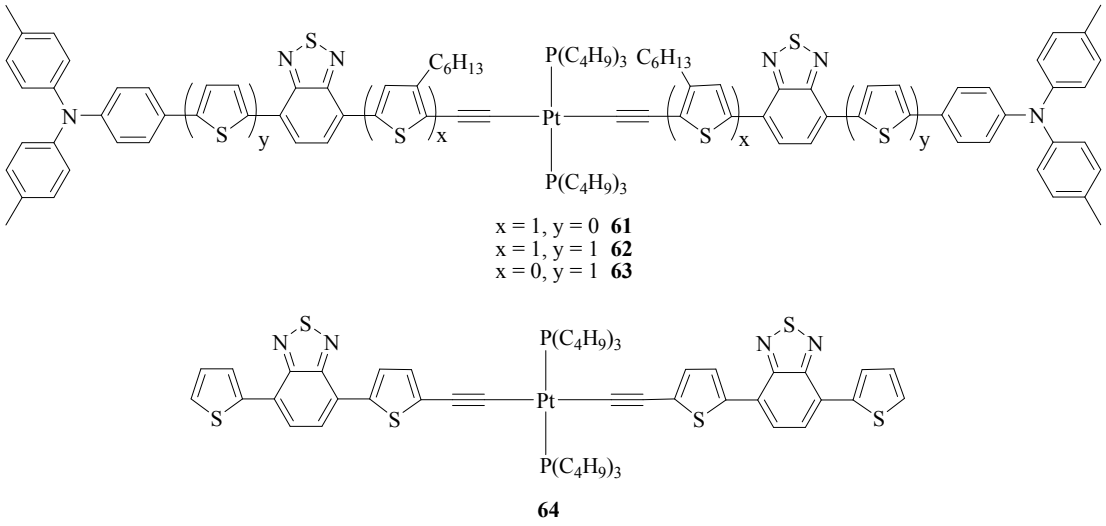

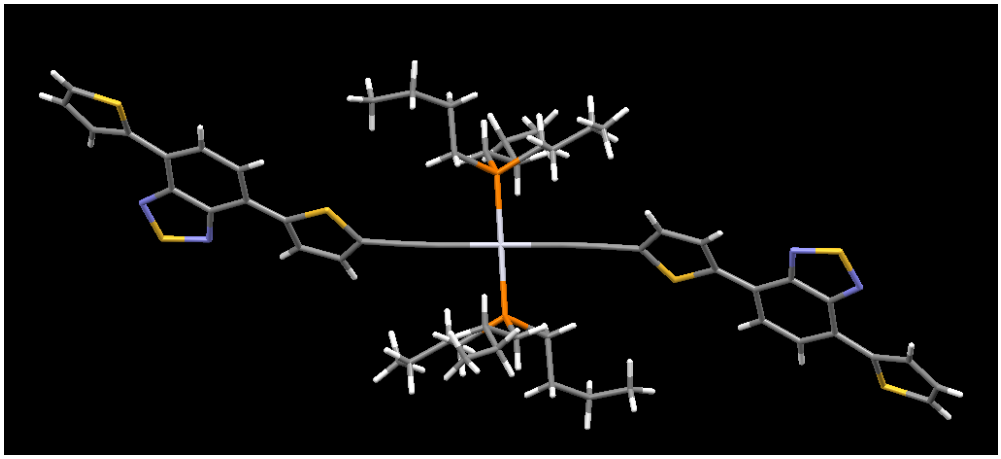

Fig. 8. X-ray crystal structure of **64**.

A new type of Pt-bis(acetylide) small molecules with an unconventional roller-wheel shaped structure **65**−**67** was recently prepared which contrasts with the traditional Pt-bis(acetylide) polymers and small molecules possessing the dumbbell design [61, 62]. The E_g of **65** (1.97 eV) and **66** (1.94 eV) are lower than that of **67** (2.53 eV). This new structural model allows partial overlap among adjacent chromophores through a slip-stack fashion, leading to higher crystallinity and charge

mobility. The X-ray crystal structural analysis of **65** unambiguously confirms the slip-stack geometry in the solid state. The structure-property relationship of such roller-wheel Pt-containing molecules was also elucidated in detail. Transient absorption measurements and theoretical calculations indicate long-lived triplet states in these molecules showing both π-π* and ICT characters. The BHJ devices based on **66** gave an impressive PCE of 5.6% (V_{oc} = 0.82 V, J_{sc} = 11.9 mA cm^{-2}, FF = 0.57) which is among the highest reported to date for Pt-acetylide compounds. However, the PCEs are very sensitive to optimization conditions and blend morphologies, which depend on the materials crystallinity, phase separation and the relative positions of the lowest singlet and triplet excited states. Results indicate that the degree of crystallinity of the materials is a key to the OSC performance. Compound **66** is less crystalline than **65** due to the shorter roller lengths, which can provide a wider window for optimization and lead to the optimized morphologies after solvent vapor annealing as well as higher PCE for **66**. By comparing **66** with **67**, complex **66** showed much reduced E_g and enhanced intermolecular interactions, leading to its better photovoltaic behavior.

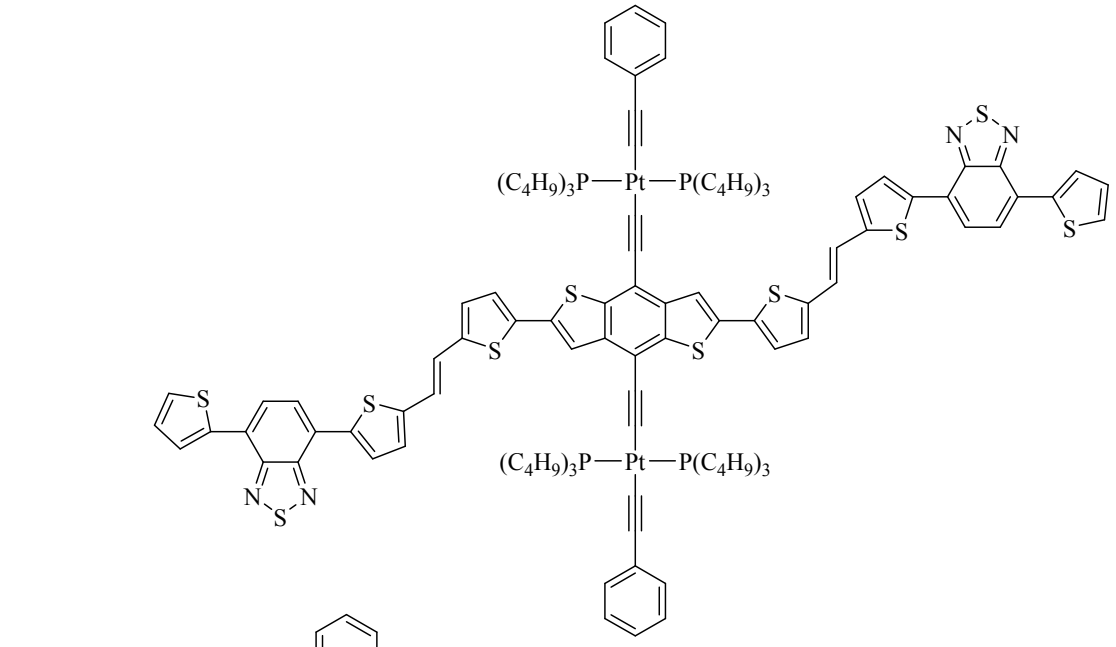

65

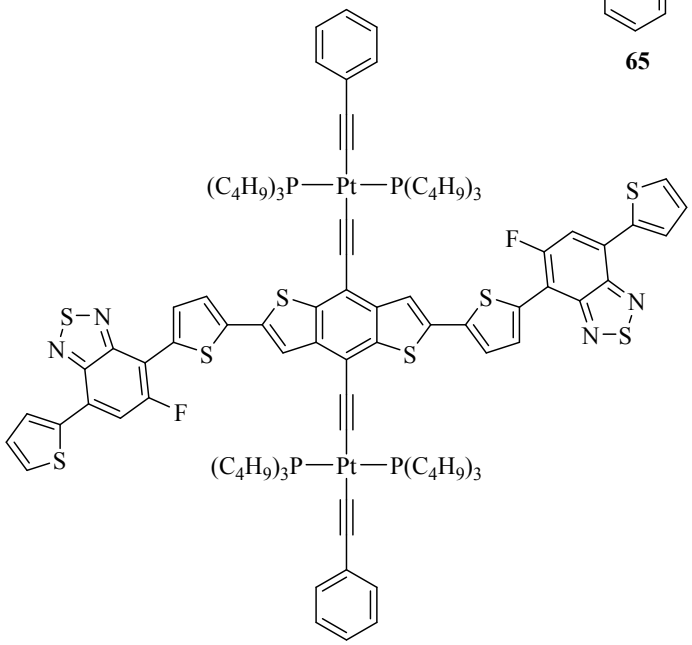

66

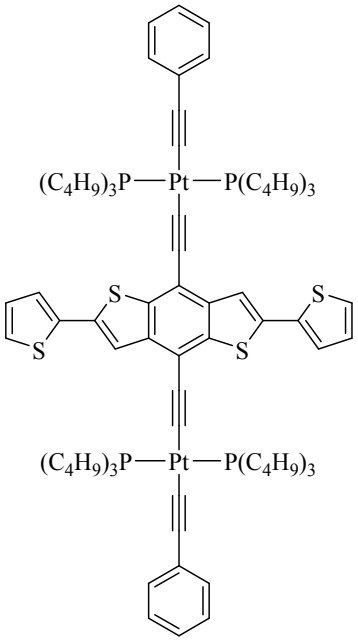

67

Dye-sensitized solar cells (DSSCs) represent one of the most promising types of organic solar cells to date. Many leading reviews are available in the literature that describe the structure and working mechanism of a DSSC [63−67]. However, for the

sake of general readers and new researchers in this area, the basic structure of the device is also shown in brief here (Fig. 9). A typical DSSC consists of two glass plates coated with a transparent conductive oxide layer. The working electrode is covered with a film of a dye-sensitized substance and the counter electrode is coated with a catalyst. Both plates are sandwiched together with the gap between them filled by an electrolyte. Light absorption is carried out by the dye molecules in which the absorbed photons cause photoexcitation of the dye to release an electron rapidly to the semiconductor. The injected electrons then hop through the colloidal TiO_2 particles to reach the collector. Following this, the electron passes through an outer circuit to reach the other transparent conductive oxide layer at the counter electrode, ultimately doing electrical work. Finally, the electron is then transferred to the electrolyte where it reduces the oxidant and the reduced form reduces the excited dye to the ground state and completes the circuit. In these types of cells, Ru(II)-bipyridine dyes have played a prominent role and organometallic complexes of other transition metals including Cu(I), Re(I), Os(II) and Ir(III) have attracted increasing attention in recent years [64, 68−70].

Pt(II)-based bis(aryleneethynylene) complexes of the unsymmetrical structural type D-π-M-π-A (M = metal) can also be made to function as photosensitizing dyes for DSSC implementation. Complexes **68**−**75** are some good examples of this design

[71]. Their absorption, electrochemical, impedance spectroscopic and photovoltaic properties were characterized in detail, which were also supported by computational studies using TD-DFT. For dyes **68**−**71**, the peak absorption wavelength can be tuned toward low-energy side up to 650 nm by using triphenylamine and/or thiophene electron−donating group. Photosensitizers **68** and **70** gave the PCE of 1.56 and 1.57%, respectively. Tian et al. also reported a simple dye **72** which can boost up the PCE to 3.28% [72]. Wong and co-workers later on prepared some phenothiazine-based Pt-bis(acetylide) dyes **73**−**75** with different donor units and respectably high PCEs in the range of 4.34−5.78% can be achieved [73]. DSSC based on dye **73** produced the highest PCE of 5.78% with a significantly high V_{oc} of 0.74 V. The good performance is mainly attributed to the high resistance to the recombination of electrons. This agrees with the Nyquist plots and Bode plots of electrochemical impedance spectrum under dark conditions. From the results obtained, it was shown that changing the position of the alkoxy chain would not modulate the absorption, HOMOs/LUMOs and their energy levels to a large extent. The differences in the PCE are mainly attributed to their differences in electron lifetime and charge-transfer resistance, and these two effects are governed by the position of the alkoxy chain. This concept thus provides a new venture to afford a novel class of bipyridine-free metal complexes for DSSCs.

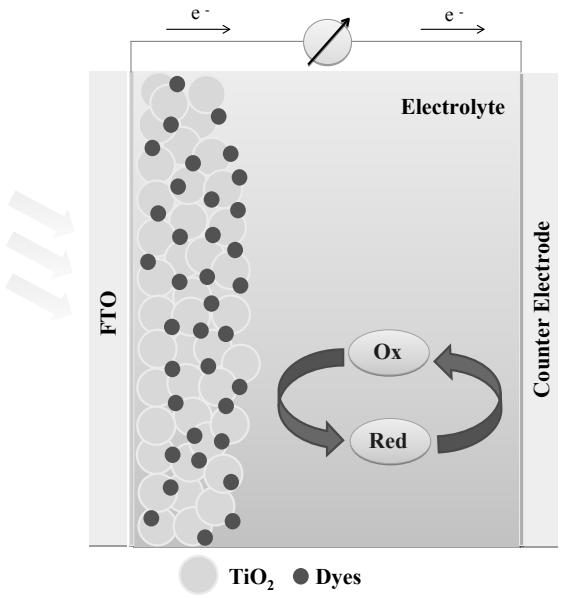

Fig. 9. A typical structure of a DSSC.

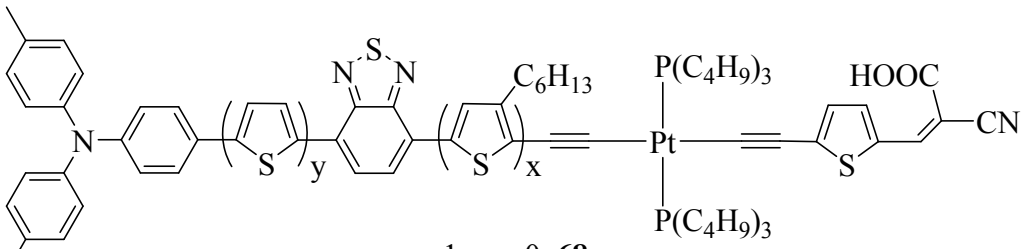

x = 1, y = 0 **68**
x = 1, y = 1 **69**
x = 0, y = 1 **70**

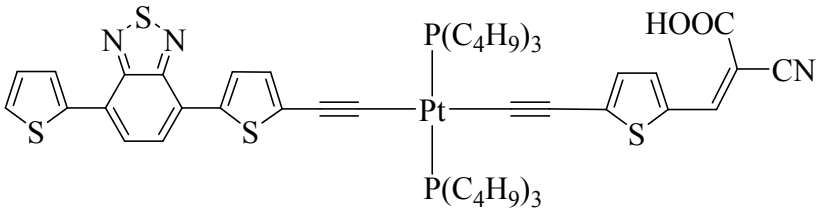

71

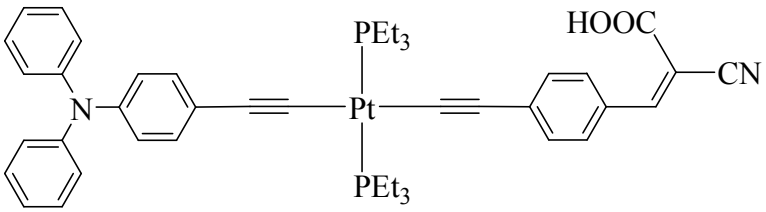

72

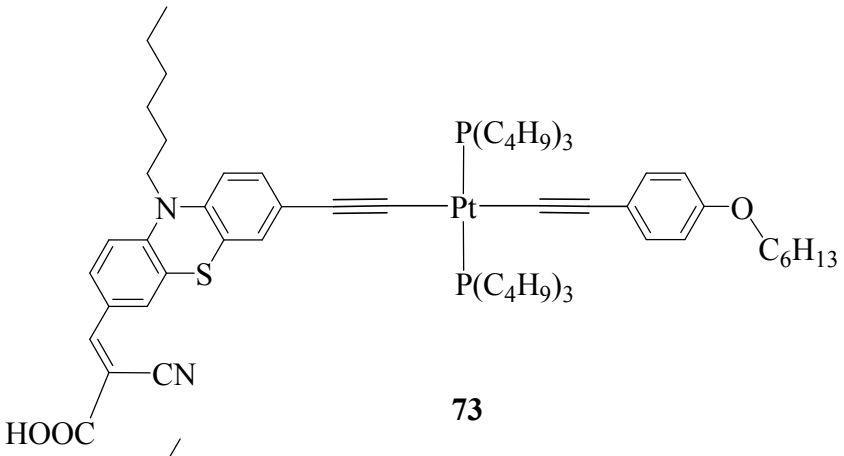

73

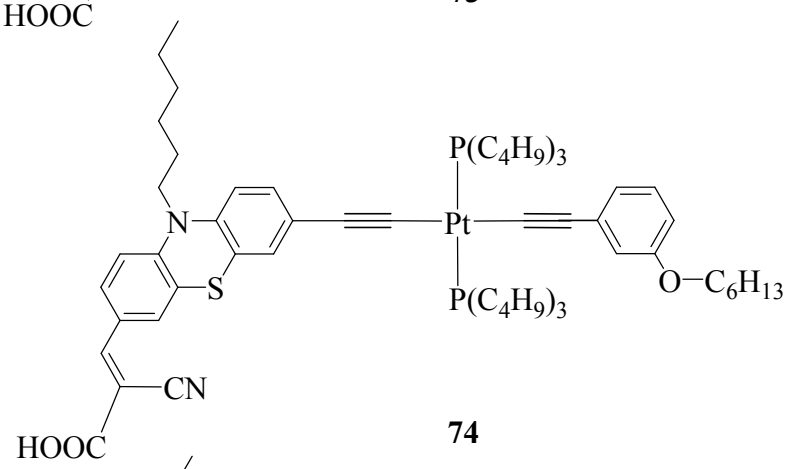

74

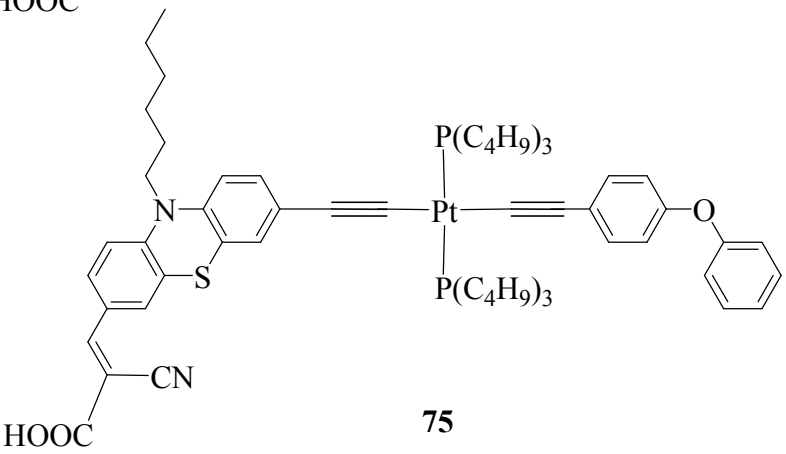

75

Polyyne materials containing fullerene units can show efficient charge separation and good photovoltaic response in pure solid materials. Schanze's group developed a D−A triad by covalently linking a Pt-acetylide oligomer to two C_{60}-based acceptors in **76** [74]. Electrochemical scans of **76** showed four reversible redox waves; the anodic waves were attributed to the oxidation of the Pt-acetylide group, and the three

cathodic waves was due to the reduction of the two fulleropyrrolidine moieties. Such triad would increase the photoinduced electron transfer (PET) efficiency and reduce the spatial separation of the D and A phases in BHJs. This approach identifies the role of triplet-state involvement in organometallic photovoltaics. The absorption profile of **76** is a linear sum of those from **76a** and C_{60} moieties. The triplet state of Pt-acetylide in the triad **76** is efficiently quenched, presumably via intramolecular PET to C_{60} (C_{60}–^{3}[**76a**]*–C_{60} → C_{60}–[**76a**$^{+\bullet}$]–$C_{60}^{-\bullet}$), suggesting that triplet state is active in charge generation. Photoexcitation of the **76a** unit in **76** is followed by very fast PET to produce the charge-separated state consisting of a mixture of singlet and triplet spin-states. A solar cell based on neat **76** provided a moderate PCE of 0.05% (IPCE ~22%) with V_{oc} = 0.41 V, J_{sc} = 0.5 mA cm^{-2} and FF = 0.28, which outperformed individual solar cells made with **76**:PCBM and **76a**:PCBM blends. The results revealed that hole and electron transport were efficient in **76**.

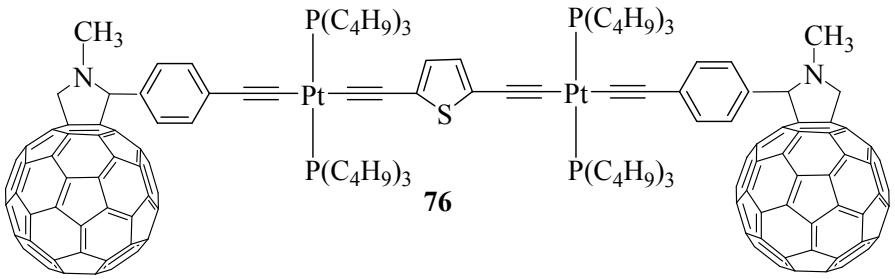

76

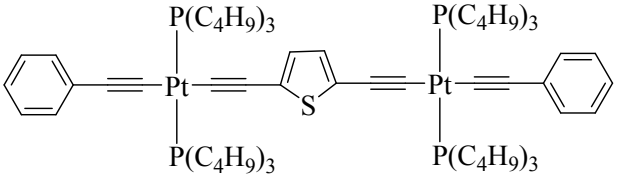

76a

Table 1

Summary of frontier energy levels and photovoltaic properties of various polyplatinaynes.

Polymer	Optical bandgap [eV]	HOMO/LUMO [eV]	V_{oc} [V]	J_{sc} [mA cm^{-2}]	FF	PCE [%]	Ref.
2	2.80	-/-	0.64	0.99	0.43	0.27	[21]
5	1.85	−5.37/−3.14	0.82	15.43	0.39	4.93	[37]
6	1.84	−5.53/−3.63	0.50	4.56	0.35	0.78	[40]
7	1.84	−5.18/−3.34	0.84	7.33	0.39	2.69	[41]
8	1.82	−5.12/−3.30	0.81	8.67	0.51	3.57	[41]
9	1.81	−5.14/−3.33	0.79	9.61	0.49	4.13	[41]
10	2.06	−6.09/−3.31	0.80	4.00	0.34	1.09	[42]
11	1.85	−5.78/−3.46	0.78	4.94	0.42	1.61	[42]
12	1.97	−5.19/−2.95	0.66	2.99	0.34	0.68	[43]
13	1.54	−4.82/−3.11	0.52	2.71	0.26	0.36	[43]
14	1.66	−4.96/−3.03	0.53	2.14	0.28	0.32	[43]
15	1.50	−5.46/−3.96	0.55	2.04	0.34	0.37	[43]
16	1.47	−5.40/−3.89	0.50	2.90	0.38	0.56	[43]
17	1.50	−5.44/−3.96	0.52	2.61	0.31	0.42	[44]
20	1.54	−5.50/−3.96	0.66	4.95	0.31	1.02	[45]
21	1.65	−5.51/−3.86	0.72	2.99	0.36	0.78	[45]

22	2.46	−5.91/−3.51	0.73	0.91	0.32	0.21	[47]
23	2.28	−5.82/−3.64	0.83	2.33	0.39	0.76	[47]
24	2.22	−5.79/−3.69	0.81	6.93	0.38	2.14	[47]
25	2.19	−5.71/−3.65	0.88	6.50	0.44	2.50	[47]
26	2.93	−5.88/−3.86	0.74	1.22	0.37	0.33	[48]
27	2.60	−5.85/−3.87	0.95	2.50	0.58	1.36	[48]
28	2.43	−5.79/−3.87	0.94	4.05	0.56	2.11	[48]
29	2.33	−5.73/−3.89	0.89	6.59	0.41	2.41	[48]
31	2.66	−5.56/−2.87	0.76	3.70	0.37	1.03	[49]
32	2.52	−5.51/−3.00	0.78	4.00	0.39	1.27	[49]
33	1.53	−5.57/−3.88	0.71	1.65	0.29	0.34	[50]
34	1.44	−5.44/−3.89	0.68	3.15	0.34	0.74	[50]
35	2.34	−6.25/−3.91	0.58	1.44	0.33	0.28	[51]
36	2.28	−6.13/−3.85	0.53	2.67	0.28	0.39	[51]
37	2.30	−6.06/−3.76	0.70	0.14	0.20	0.03	[52]
38	1.88	−5.96/−3.78	0.78	1.40	0.32	0.35	[52]
39	2.72	−5.50/−2.78	0.74	2.99	0.38	0.83	[53]
40	2.68	−5.49/−2.81	0.76	4.79	0.44	1.60	[53]
41	2.59	−5.67/−3.08	0.82	4.09	0.53	1.78	[53]

42	1.68	−5.19/−3.07	0.52	0.86	0.25	0.11	[44]
43	1.89	−5.23/−3.09	0.64	2.35	0.20	0.31	[44]
44	1.88	−5.20/−3.17	0.68	4.21	0.25	0.71	[44]
45	1.55	−4.96/−3.11	0.50	1.39	0.23	0.16	[44]
46	1.54	−4.94/−3.14	0.50	0.99	0.23	0.11	[44]
47	1.53	−5.12/−3.28	0.32	0.17	0.18	0.009	[44]

Table 2

Summary of frontier energy levels and photovoltaic properties of small-molecule Pt(II) metallaynes.

Molecule	Optical bandgap [eV]	HOMO/LUMO [eV]	V_{oc} [V]	J_{sc} [mA cm^{-2}]	FF	PCE [%]	Ref.
54	1.90	−5.29/−3.35	0.71	7.91	0.42	2.30	[58]
55	1.90	−5.28/−3.38	0.82	8.54	0.43	3.00	[58]
56	1.90	−5.29/−3.38	0.73	7.66	0.40	2.20	[58]
57	1.76	−5.40/−3.50	0.91	3.61	0.28	0.88	[59]
58	1.69	−5.37/−3.49	0.93	5.89	0.29	1.59	[59]
59	1.88	−5.39/−3.56	0.60	1.22	0.34	0.17	[59]
60	1.91	−5.27/−3.57	0.92	4.88	0.33	1.56	[59]
61	2.06	−5.10/−3.00	0.83	7.10	0.40	2.37	[60]
62	1.93	−5.03/−3.13	0.80	7.15	0.41	2.34	[60]
63	2.09	−5.07/−2.96	0.81	4.99	0.36	1.45	[60]
64	2.11	−5.21/−3.08	0.86	2.44	0.26	0.54	[60]
65	1.97	−4.90/−3.20	0.79	11.2	0.36	3.2	[62]

66	1.94	−5.0/−3.2	0.82	11.9	0.57	5.6	[61, 62]
67	2.53	-/-	0.35	0.06	0.50	0.01	[62]
68	1.80	−5.26/−3.46	0.62	3.60	0.70	1.56	[71]
69	1.47	−5.11/−3.64	0.58	3.35	0.73	1.42	[71]
70	1.69	−5.19/−3.50	0.59	3.63	0.73	1.57	[71]
71	1.45	−5.03/−3.58	0.57	2.14	0.66	0.80	[71]
72	2.48	−4.84/−2.36	0.70	6.77	0.69	3.28	[72]
73	2.23	−5.70/−3.47	0.74	10.98	0.71	5.78	[73]
74	2.22	−5.65/−3.43	0.69	8.99	0.71	4.43	[73]
75	2.27	−5.62/−3.35	0.70	8.75	0.71	4.34	[73]

3.2. Metalloporphyrins of zinc(II) with acetylide linkers

Research on OSCs is progressing at a rapid pace and it is still a great challenge to design efficient metalated compounds with long-term stability and low production cost. It is envisioned that most of the porphyrin-functionalized polymers would contain an extensively conjugated 2D π-system, high mobility and extended optical absorption, which render them suitable for use as the photoactive layer for OSC application. Below summarizes some recent examples of acetylide-functionalized metalloporphyrin-containing polymers and the key device parameters are collated in Table 3. By comparing the triple-bond linked polymer **77** with the single-bond linked congener **77a**, polymer **77** was electrochemically active in both the oxidation and

reduction regions, whereas the polymer **77a** displayed only an oxidation wave. The red-shifted absorption and stronger Q-band of **77** in the thin film was believed to be due to the aggregation caused by a more coplanar main chain. By virtue of the more coplanar and extended π-conjugated main chain, stronger aggregation and intermolecular interactions in the solid state for **77**, it gave a higher hole mobility than **77a** at room temperature. This is also in agreement with the higher PCE for the more rigid **77** than **77a** [75], thanks to the stronger Q-band absorption and higher mobility observed for **77**. Similar phenomenon was also observed for an acetylene-containing perylene diimide copolymer relative to the conjugated counterpart without acetylene spacers [76].

Typical porphyrin-based absorption profiles can be observed for all metalloporphyrin-containing polyplatinayne polymers **78**−**80**, which display a sharp and strong Soret band at about 430 nm and a set of weak Q bands between 540 and 635 nm [77]. This type of polymers does not display significant π-conjugation because the large aryl-porphyrin dihedral angles, which result from steric interactions with the β-hydrogens, lead to the non-planarity. The substituent effect of the thiophene residue onto the π-π* type transitions of the Zn(II) prophyrin unit in **80** results in more red-shifted Soret band and Q-bands by 10−15 nm as compared to **78**. The E_g for these polymers vary from 1.93 to 2.02 eV, and the lower E_g in **79** than **78**

favors harvesting of more solar photon energy (Table 3). Owing to the stronger absorption features with a broader Soret band and stronger Q-bands in **80**, its OSC exhibited the highest PCE of 1.04% with V_{oc} of 0.77 V, J_{sc} of 3.42 mA cm^{-2} and FF of 0.39.

To date, the search of the best D−A copolymer systems to achieve high PSC performance is usually hampered by the fact that the adjustment in the molecular structures of D and A units often leads to undesirable trade-off among the parameters V_{oc}, J_{sc} and FF. Normally, reduction of E_g of a D−A copolymer favors higher J_{sc}, but it could be accompanied by the elevation of the HOMO energy level and the drop of V_{oc}. Maintaining V_{oc} while decreasing E_g is also a challenging issue since shifting the LUMO energy downward decreases the LUMO-LUMO offset and affects the charge transfer efficiency between the polymer donor and the accepter. By attaching a porphyrin-pyrene pendant as a complementary light harvesting unit, the two-dimensional D−A copolymers **81**−**82** were prepared by Hsu et al., which serve as a panchromatic absorber (Fig. 10) [78]. The two 2,6-bis(dodecyloxy)phenyl substituents on the porphyrin ring prevents strong aggregation of the light harvesting unit. With such copolymerization strategy to circumvent the above trade-offs, the PCE of 8.0% was obtained in an additive-free PSC which can be further improved to 8.6% when 5 vol% of 1-chloronaphthalene was used as a processing additive and

[6,6]-phenyl-C_{61}-butyric styryl dendron ester was used as a cathodic interlayer. Relative to the organic copolymer **81a** without such porphyrin side chain, the PCE was only 6.8%.

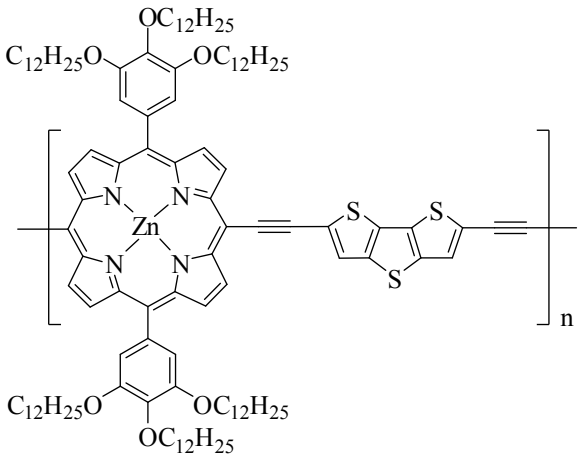

77

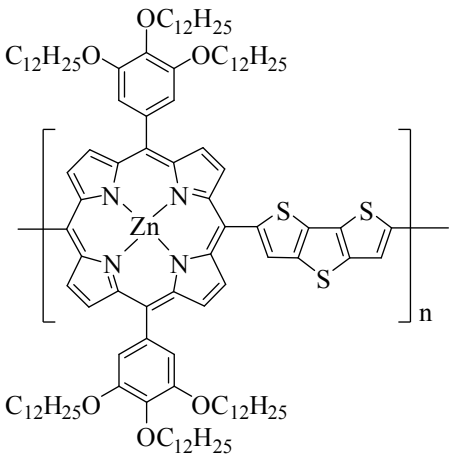

77a

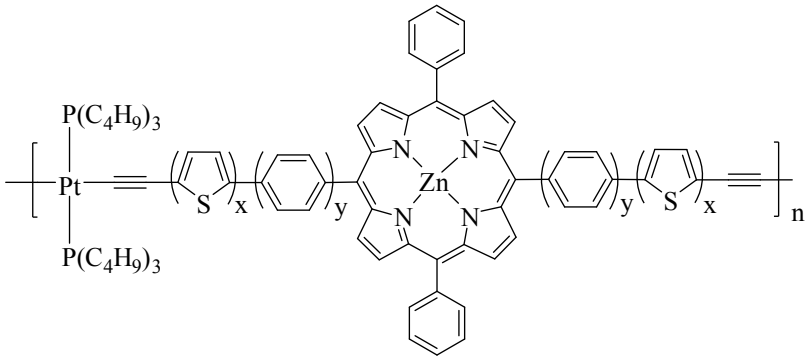

x = 0, y = 1 **78**
x = 1, y = 1 **79**
x = 1, y = 0 **80**

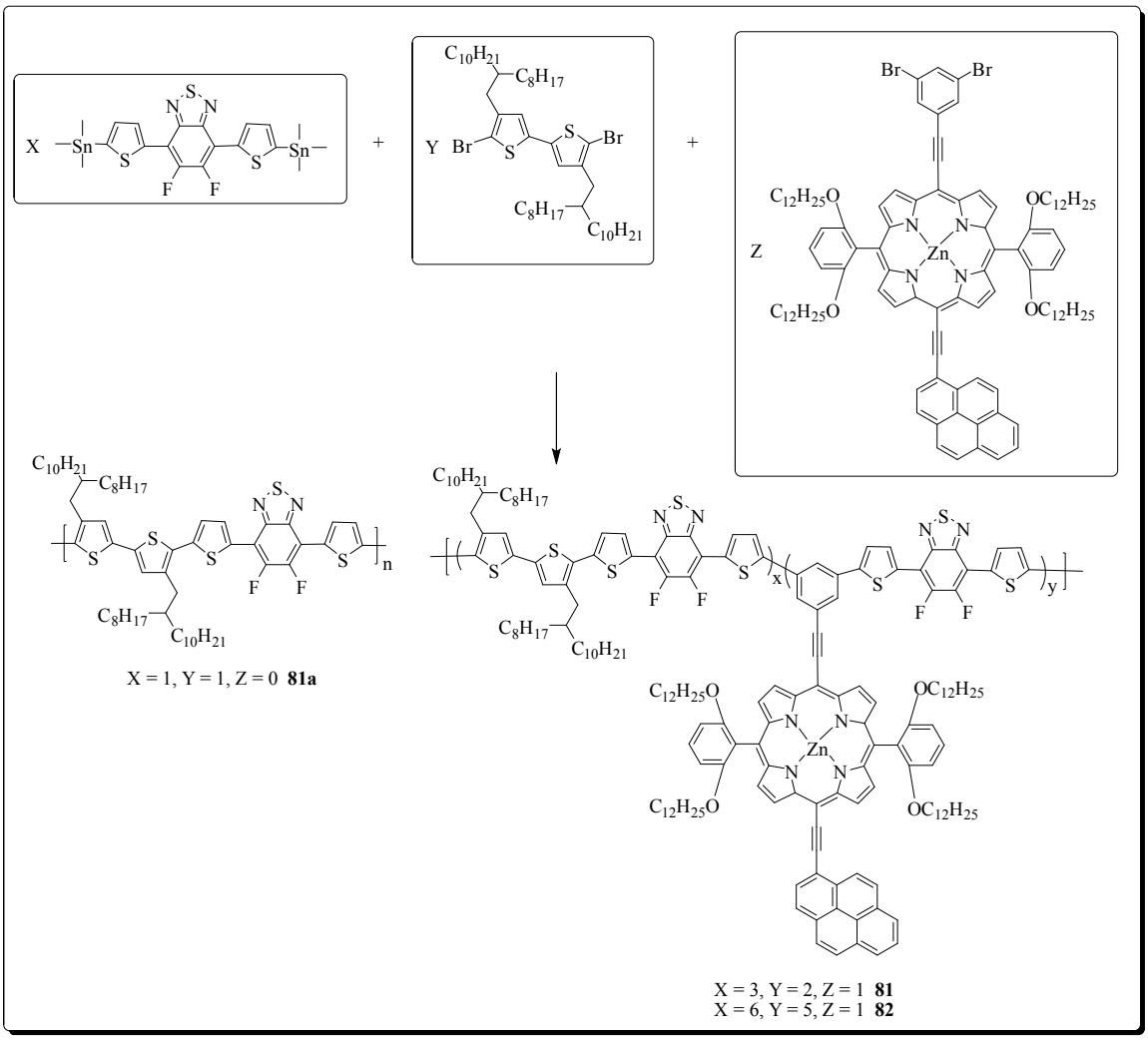

Fig. 10. Synthesis of two-dimensional D−A copolymer **81**−**82** and the structure of the organic analogue **81a**.

Porphyrin-based molecular structures play a key role in solar energy research. Porphyrins have drawn immense attention as photosensitizers owing to the large absorption coefficients of their Soret and Q bands in the visible region. Inspired by the efficient energy transfer in naturally occurring photosynthetic reaction centers, numerous porphyrins have been developed for organic solar cells. In this section, a

library of A-π-D-π-A Zn(II)-porphyrin small-molecule donor materials **83**–**97** were developed for solution-processed BHJ solar cells with good photovoltaic performance (Table 4). Solution-processable small molecules for BHJ OSCs are very attractive nowadays due to the proven advantages such as their defined molecular structure and molecular weight, high purity and less batch-to-batch variations as compared to their polymeric counterparts. These features hold great promise for low-cost and large-scale commercialization applications.

A conjugated Zn(II) porphyrin small molecule with dicyanovinyl-substituted thiophene groups at the *meso* positions **83** was reported which showed a broad and intense absorption in the visible and NIR regions [79]. BHJ solar cells comprising the **83**:$PC_{71}BM$ layer fabricated using THF solvent gave a PCE of 3.65% and the PCE can be improved to 5.24% by using a mixture of 4 vol% pyridine-THF instead. The enhancement in the J_{sc} and FF values is the outcome of the stronger and broader IPCE response and reduced domain sizes in the active layer, which causes a more balanced charge transport, and enhanced hole mobility in the device. Peng and co-workers have developed a series of promising conjugated A-π-D-π-A porphyrin-based donors **84**–**89** for BHJ applications. The absorption spectrum of **84** in thin film versus that in solution revealed a red-shift of 35 nm at the Q band region, which was due to the strong intermolecular interaction in the solid state, hence leading to a low E_g of 1.3

eV. By comparing the triple-bond linked complex **84** with **84a** without the acetylene linkages, there is a substantial improvement in the hole mobility and photovoltaic performance from **84a** to **84** (μ_h = 7.4 × 10^{-6} cm^2 V^{-1} s^{-1} and PCE = 4.02% for **84** versus μ_h = 2.5 × 10^{-9} cm^2 V^{-1} s^{-1} and PCE = 0.71% for **84a**) [80]. This is believed to be caused by the more efficient π-electron conjugation and thus the delocalized π-electrons in **84** and the more efficient ICT process. This is consistent with the density functional theory (DFT) calculations which shows that **84** is planar and the π-electrons are delocalized in the whole molecule both at the HOMO and LUMO. For **84a**, the BTD rings are almost perpendicular to the porphyrin plane and the π-electrons are almost confined to the porphyrin ring at the HOMO and to BTD at the LUMO. As a result, the coplanarity of the units in **84** allows the molecule to be fully conjugated and the π-electrons to be delocalized along the whole molecule. Later on, a few Zn(II) porphyrin donor molecules with DPP acceptor end groups **85**−**89** were also reported. The effects of N-substituent chain length on DPP, additive and morphology control on the PCE of these donors were investigated. BHJ devices made from **85**:PCBM (1:1, w/w) showed PCE of 3.71% and μ_h of 7.4 × 10^{-6} cm^2 V^{-1} s^{-1}, which were further enhanced to 4.78% and 1.6 × 10^{-4} cm^2 V^{-1} s^{-1} after addition of 3.0 vol% of pyridine additive [81]. A small amount of pyridine additive could result in a better interpenetrating network by preventing the active layers from undergoing large-

scale phase separation, a more balanced charge transport and a slight crystallinity enhancement. The replacement of 3,5-di(dodecyloxy)phenyl groups in **85** by 4-octyloxyphenyl groups in **86** is also a good strategy to improve the photovoltaic performance [82]. The molecule **86** with less bulky substituents at the porphyrin periphery can be used to fabricate BHJ OSCs to give the best PCE up to 7.23% with a V_{oc} of 0.71 V, a J_{sc} of 16.0 mA cm^{-2} and a FF of 0.64 after the treatment with 0.4% 1,8-diiodooctane (DIO) additive. The switch of the donor from **85** to **86** and the use of the DIO additive both improve the hole transport in the devices. This improvement is attributed to the more efficient intermolecular π-π stacking of **86** and more favorable surface morphology in film. Another series of porphyrin-DPP-based small molecular photovoltaic molecules possessing 2-ethylhexyl, 2-butyloctyl and 2-hexyldecyl chains on DPP **87**−**89** was also studied and tested for high-performance BHJ OSCs [83]. A very low energy loss was observed for these materials, and hence a high V_{oc} (0.71−0.88 V) can be obtained. It was found that there is a chain-length dependence of the device efficiency on the crystalline structure and phase separation. The optimal device was obtained when **88**:PCBM blend was used as the active layer in the presence of 0.4 vol% DIO and 0.4 vol% pyridine, leading to the best PCE of 9.06%. Here, a mixed additive approach, by adding a low-volatility bad solvent to pyridine, was adopted, which created a multi-length-scale crystalline morphology, consisting of

donor material crystalline domains and acceptor aggregate domains via a single-step process. More importantly, complex **88** can be employed in the fabrication of solution-processed all-small-molecule tandem solar cells in combination with an organic donor showing a complementary absorption profile, leading to the highest PCE of 12.50% [84]. It is nice to see that the performance of the tandem cells did not change much with different thicknesses of both the front and rear subcells and under different light intensities. These results highlight the potential of small-molecule-based tandem cells as a competitive alternative in the guest for future commercialized OSCs.

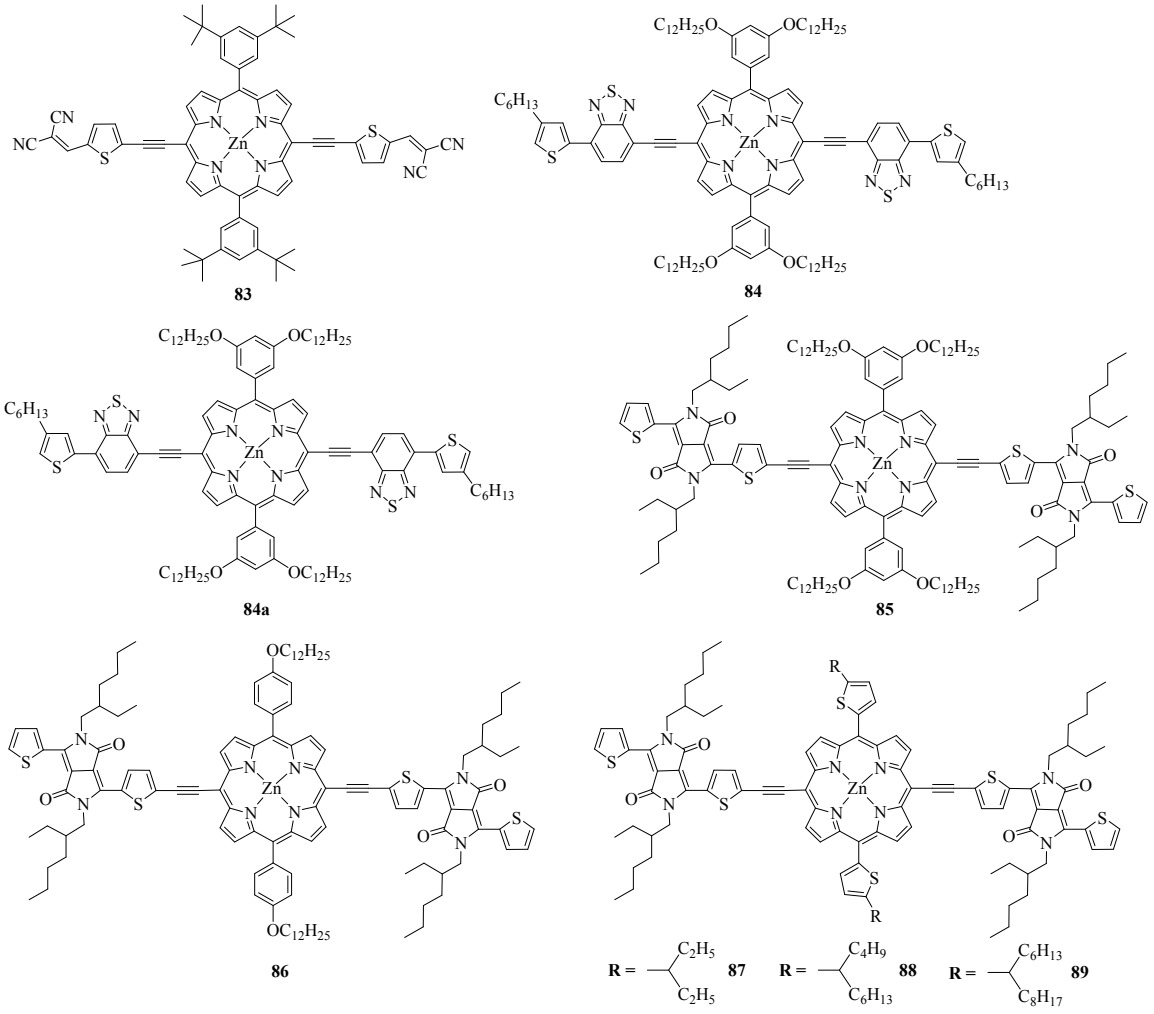

Recently, Zhu and Wong and co-workers have been engaged in the development of some porphyrin-based small molecules **90**−**97** as donors for highly efficient OSCs. Complexes **90**−**93** are constructed from *meso*-alkyl substituted porphyrins as the central core and 3-ethylrhodanine as the end groups whereas aromatic peripheral substituents are attached to the porphyrin ring instead for **94** and **95** [85, 86]. In each case, there is no significant change in the porphyrin absorption patterns due to minor electronic perturbations from *meso*-aliphatic or aromatic substituents (Fig. 11). The effect of the branching point of the alkyl chains as well as the aromatic substituent on

the film morphology, charge mobility and photovoltaic performance has been studied for **90**−**95**. Among them, careful structural engineering of these small molecules can promote stronger intermolecular π-π stacking and higher charge mobility in the film, eventually resulting in the best PCE of 7.70% in a conventional BHJ device based on **93** (Fig. 12). The inverted BHJ devices have also been tested which showed long-term ambient stability with comparable PCE of 7.55%. Later on, two related porphyrins **96** and **97** bearing terthiophene bridges were also utilized for OSCs [87]. In this study, the horizontal conjugation of 3,3”-dihexylterthiophene to the porphyrin ring with the vertical aliphatic 2-octylundecyl peripheral substituents can effectively increase the solar flux coverage between the conventional Soret and Q bands of the porphyrin core and optimize the molecular packing through polymorphism associated with side chains and the linear π-conjugated backbones. The best PCE was achieved for **97** at 8.21% with V_{oc} of 0.82 V, J_{sc} of 14.30 mA cm^{-2} and FF of 0.70.

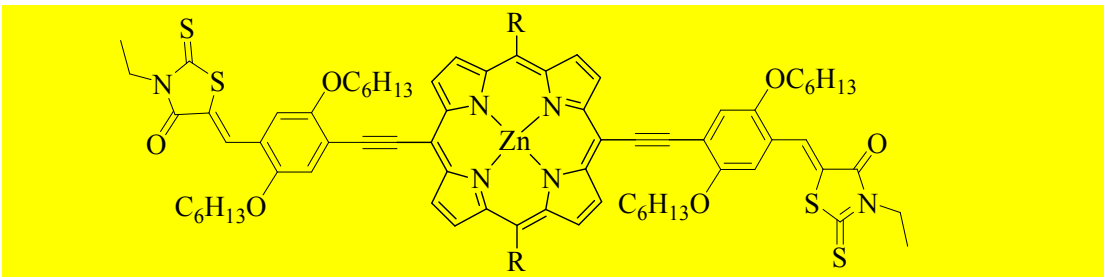

R = 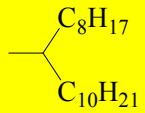 **90** 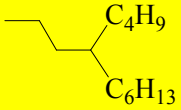 **92** 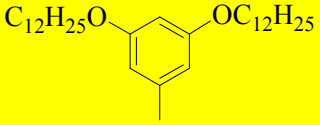 **94**

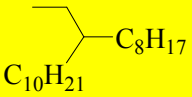 **91** 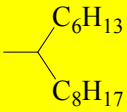 **93** 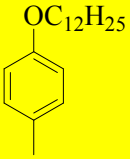 **95**

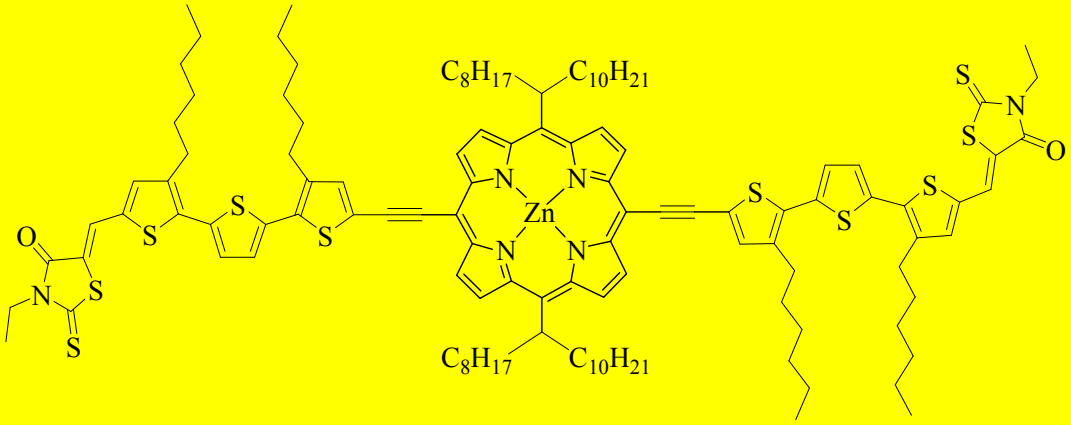

96

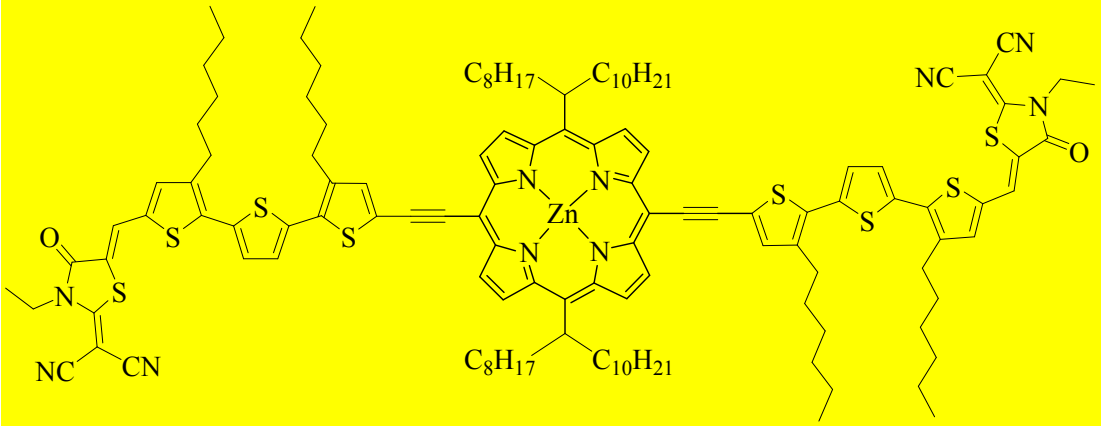

97

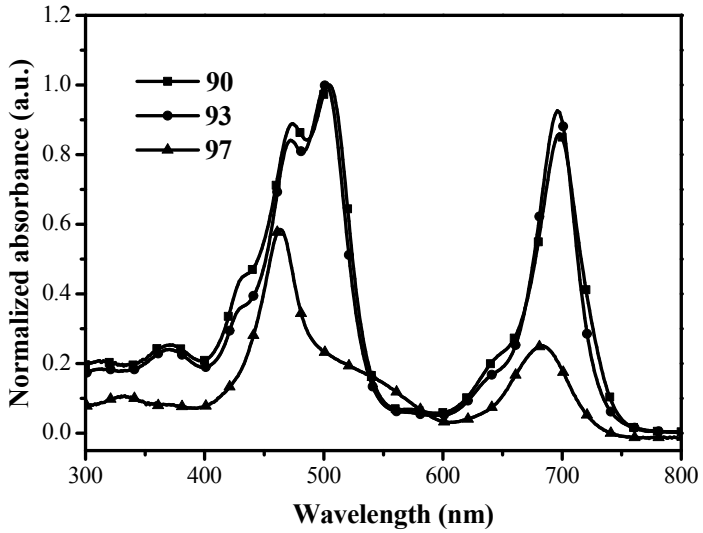

Fig. 11. Absorption spectra of **90**, **93** and **97**.

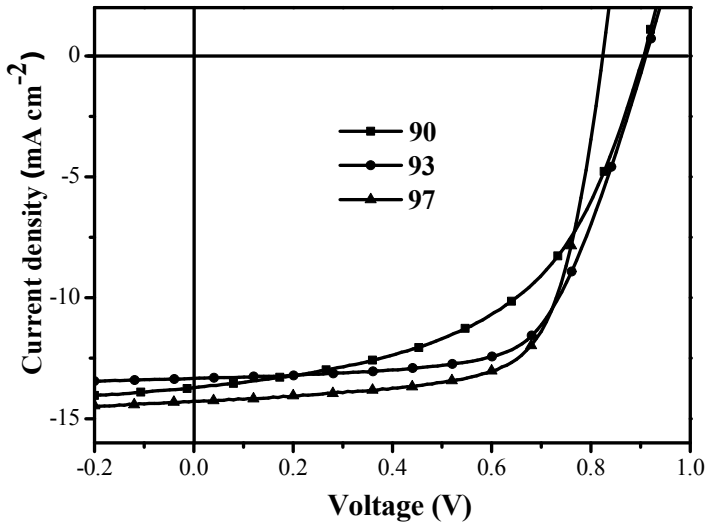

Fig. 12. *J*−*V* curves for the BHJ devices made from **90**, **93** and **97**.

Photosensitizer is the central component of DSSCs, which harvests sunlight and produces excited electrons at the semiconductor interface for current generation. Triarylamine and its derivatives possess strong light-capturing and electron-donating abilities, which favor the enhancement of direct electron-injection efficiency and have

been proven to be an excellent candidate as electron donor segment in the photosensitizer [65]. Numerous examples of D-π-A structured Zn(II) porphyrins **98**−**106** are highlighted here. In the first place, three related dyes **98**−**100** were designed and compared for DSSC performance evaluation [88]. By inserting a thienyl ring between the porphyrin ring and the electron-withdrawing benzoic acid unit, the short-wavelength absorption peak maximum was red-shifted from 459 nm (**98**) to 466 nm (**99**) and 471 nm (**100**) whereas the long-wavelength peak from 667 nm (**98**) to 674 nm (**99**) and 678 nm (**100**). Fast interfacial charge recombination was observed when the anchoring group was changed from benzoic acid in **99** to cyanoacetic acid in **100**. DSSCs fabricated from **99** and **100** gave good PCE at 7.8 an 6.1%, respectively, against the $[Co(bpy)_3]^{2+/3+}$ redox electrolyte (bpy = 2,2'-bipyridine). Factors governing the photovoltaic performance was also examined by transient photovoltage decay measurements. Dyes **101**–**106** employing triarylamine as the donor group and the ethynylbenzoic acid moiety as the acceptor unit have been found to be very favorable for DSSC applications. The porphyrin chromophore itself constitutes the π-bridge in such particular D-π-A structure. Dye **101** showed typical absorption bands of the porphyrins, which absorbs light over the whole visible range, viz., an intense Soret band at ca. 460 nm and a series of lower intensity Q bands at longer wavelengths (550–700 nm) [89]. **101**-based DSSCs with a double layer TiO_2 film

gave a PCE of 11% with iodide/triiodide redox shuttle in the electrolyte. To impair the interfacial back electron reaction in such D-π-A porphyrin-based structure and to produce a striking amelioration of the photoinduced charge separation in DSSCs, long-chain octyloxy groups are incorporated in the *ortho* positions of each *meso*-phenyl ring in **102**. Higher PCE of 11.9% was achieved using the **102** photovoltaic system and cobalt tris(bipyridyl)-based redox shuttle, which produced a V_{oc} of 0.97 V, a J_{sc} of 17.3 mA cm^{-2} and a FF of 0.71 [90]. Further co-sensitization of **102** with selected organic dyes yielded an even higher PCE of 12.3% under simulated air mass 1.5 global sunlight. The robustness of these DSSCs was also demonstrated by continued exposure of the cells for 220 hours to full sunlight, and only a small decline of the overall efficiency over the extended light-soaking period was detected, implying good cell stability. In order to fill the absorption valley between the Soret and Q bands and further broaden the absorption spectra, BTD as the π-conjugated linker was introduced in the design of **103** and **104** [91]. Owing to the strong electron-accepting nature of BTD group, a red-shift in the absorption profile was observed in **104** as compared to **102**. It was found that it is critical to introduce the phenyl group between the Zn(II) porphyrin and BTD in **105** for the enhancement of PCE. The PCE of the device based on dye **104** was measured to be 13.15% while that from **103** was 2.52% only. The electron-injection dynamics and the lifetime of the photogenerated

charge carriers were determined by using time-resolved fluorescence, transient photocurrent decay and transient photovoltage decay measurements. By engineering this prototypical structure of D-π-A porphyrins in order to maximize the cobalt-electrolyte compatibility simultaneously and to yield improved light-harvesting properties, functionalization of the porphyrin core with the bulky bis(2',4'-bis(hexyloxy)-[1,1'-biphenyl]-4-yl)amine donor was adopted in **105** and **106** [92]. The dramatically improved absorption properties of **106** resulted in a near-quantitative light-harvesting ability across the visible spectrum and in the NIR region up to 800 nm, leading to higher photocurrents in the **106**-based DSSC device as compared to **105**-based device. Without the use of an organic co-sensitizer, DSSC using the photosensitizer **106** and the cobalt(II/III) redox shuttle resulted in a highly efficient DSSCs that exhibited a V_{oc} of 0.91 V, a J_{sc} of 18.1 mA cm^{-2}, a FF of 0.78 and a PCE of 13%.

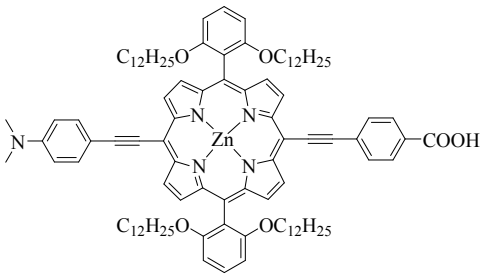

98

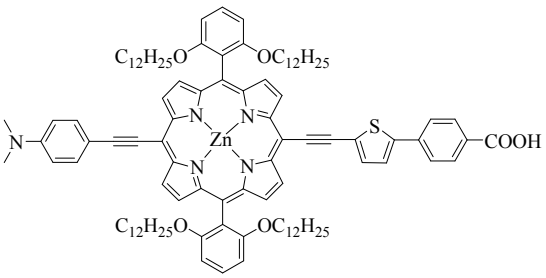

99

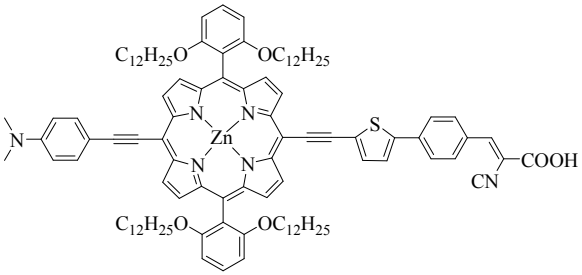

100

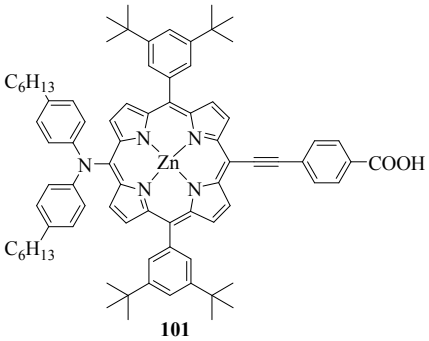

101

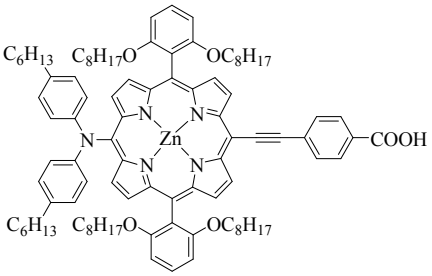

102

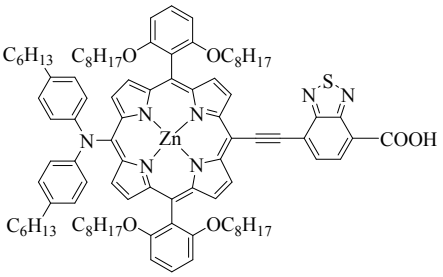

103

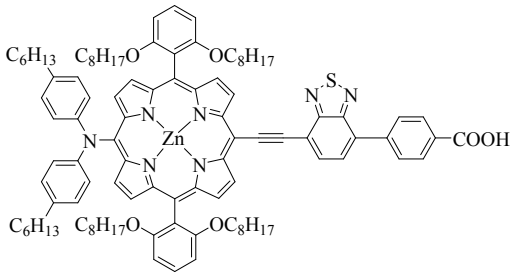

104

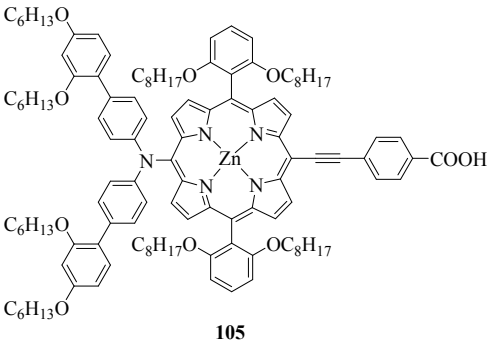

105

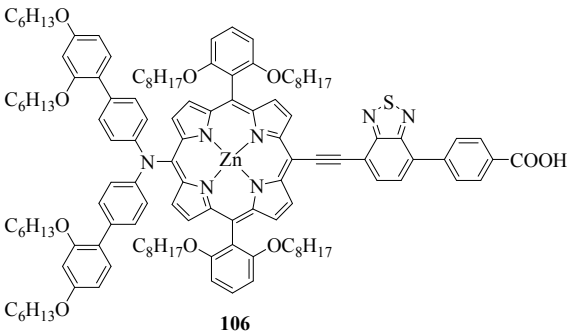

106

Table 3

Summary of frontier energy levels and photovoltaic properties of acetylide-functionalized Zn(II) porphyrin-containing polymers.

Polymer	Optical bandgap [eV]	HOMO/LUMO [eV]	V_{oc} [V]	J_{sc} [mA cm^{-2}]	FF	PCE [%]	Ref.
77a	-	−5.5/−3.6	0.45	0.45	0.29	0.06	[75]
77	-	−5.2/−3.3	0.58	1.52	0.34	0.30	[75]
78	2.02	−5.58/−3.64	0.72	2.74	0.34	0.68	[77]
79	2.00	−5.62/−3.73	0.78	3.02	0.30	0.71	[77]
80	1.93	−5.53/−3.71	0.77	3.42	0.39	1.04	[77]
81a	1.65	−5.54/−3.68	0.77	13.5	0.66	6.80	[78]
81	1.65	−5.29/−3.31	-	-	-	-	[78]
82	1.63	−5.30/−3.31	0.77	16.1	0.70	8.60	[78]

Table 4

Summary of frontier energy levels and photovoltaic properties of some highly efficient acetylide-functionalized Zn(II) porphyrin dyes.

Molecule	Optical bandgap [eV]	HOMO/LUMO [eV]	V_{oc} [V]	J_{sc} [mA cm^{-2}]	FF	PCE [%]	Ref.
83	1.58	−5.44/−3.66	0.88	10.64	0.56	5.24	[79]
84	1.30	−5.2/−3.9	0.85	9.46	0.50	4.02	[80]
84a	-	-	0.88	2.81	0.287	0.71	[80]
85	-	−5.18/−3.39	0.80	11.88	0.502	4.78	[81]
86	1.36	−5.07/−3.60	0.71	16.00	0.637	7.23	[82]
87	1.37	−5.19/−3.82	0.74	17.50	0.646	8.36	[83]
88	1.37	−5.23/−3.86	0.73	19.58	0.634	9.06	[83]
88	1.37	−5.23/−3.86	1.63	12.05	0.627	12.50	[84]

89	1.37	−5.24/−3.82	0.73	17.23	0.655	8.24	[83]
90	1.50	−5.12/−3.55	0.90	13.72	0.521	6.49	[85]
91	1.55	−5.14/−3.55	0.85	6.29	0.479	2.53	[85]
92	1.54	−5.17/−3.54	0.87	10.50	0.569	5.12	[85]
93	1.60	−5.19/−3.59	0.90	7.20	0.481	3.21	[86]
94	1.55	−5.15/−3.60	0.90	10.14	0.556	5.07	[86]
95	1.60	−5.12/−3.52	0.91	13.32	0.636	7.70	[86]
96	1.52	−5.14/−3.56	0.80	14.93	0.642	7.66	[87]
97	1.45	−5.17/−3.63	0.82	14.30	0.70	8.21	[87]
98	1.840	−4.884/−3.066	0.81	13.23	0.73	7.93	[88]
99	1.818	−4.815/−3.010	0.81	12.66	0.75	7.75	[88]
100	1.805	−4.816/−2.976	0.76	10.66	0.74	6.09	[88]
101	1.99	−4.99/−3.00	0.81	8.00	0.76	9.50	[89]
101	1.99	−4.99/−3.00	0.77	18.6	0.764	11.0	[89]
102	2.11	-4.92/−2.81	0.94	9.3	0.74	12.7	[90]
103	1.80	−4.93/−3.13	0.62	5.03	0.798	2.52	[91]
104	1.81	−4.89/−3.08	0.87	9.78	0.80	13.15	[91]
105	1.88	−4.98/−2.89	0.96	15.90	0.79	12.0	[92]
106	1.79	−4.99/−3.11	0.91	18.10	0.78	13.0	[92]

3.3. Ruthenium(II) acetylide donor molecules

Although still in its infancy, the use of metallopolyynes and their oligomers represents an innovative and challenging research area for the development of BHJ solar cells. The use of a ruthenium(II) instead of a platinum(II) center in a conjugated

backbone can red-shift the absorption spectra which results in a better sunlight harvesting. There are literature precedents of using Ru(II) complexes in BHJ solar cell development. However, examples of Ru(II)-acetylide materials for BHJ applications are rare. The first example of dinuclear acetylide donor complex **107** for BHJ OSCs was reported by Colombo et al., where two Ru atoms are separated by a bridge comprising BTD flanked on either side by 2,5-thienyl units [93]. Complex **107** showed a two-electron quasi-reversible oxidation peak at 0.06 V and a one-electron quasi-reversible reduction peak at 1.73 V. The oxidation can be ascribed to the simultaneous one-electron removal of each of the two Ru centers, which also implies the absence of either through-bonds or through space electronic communication between the two Ru atoms by the conjugated organic bridge. The reduction event occurs on the organic spacer. The authors have studied the PET process from **107** to PCBM. The fluorescence band of **107** is effectively quenched by blending with PCBM, which indicates an efficient exciton dissociation at the D-A interface by PET from **107** to PCBM. Since the singlet excited state of PCBM is slightly higher in energy with respect to the singlet of **107**, energy transfer process from **107** to PCBM can be ruled out. A BHJ device made from **107**/PCBM (1:2, w/w) blend resulted in a low PCE of 0.1% only which was presumably due to the poor morphologies of the blend (Table 5). A strong tendency to phase segregation between the Ru complex and

PCBM would cause the low photocurrent.

An interesting family of multichromophoric small molecules of Ru(II)-bis(aryleneethynylene) consisting of triphenylamine and/or thiophene as the donor and BTD as the acceptor **108**−**111** was developed [94]. These complexes absorb light strongly spanning from 300 to 700 nm and the E_g value varies within 1.70−1.83 eV. These complexes generally show planarity among the thiophene and BTD units and the two acetylene groups lie in line with the Ru(II) atom to allow maximal pπ-dπ-pπ interaction. For instance, the tricyclic push-pull di(thienyl)benzothiadiazole unit in **108** is almost coplanar with dihedral angles of 3.4° and 12° between the two thiophene rings (Fig. 13), resulting in an improved absorption. An increase in the electron-donating strength in such a push-pull conjugated system led to the broadening and enhancement of the ICT transition. Donor materials **108**−**111** can be used to fabricate solution-processed BHJ solar cells with the best PCE of 0.66%. Fig. 14 compares the absorption maximum of the Pt(II) bis(acetylide) complex **63** and the corresponding Ru(II) congener **110**. As expected, the peak maximum experiences a notable red-shift in wavelength from Pt(II) to Ru(II) center, indicating better sunlight harvesting ability of the Ru(II) complex. By comparing the symmetric complex **63** with the asymmetric one **70**, a red-shifted absorption was observed for the former case since it has a more extensive delocalization of electrons in **63**.

Some Ru(II)-diacetylide organometallic complexes **112**−**114** have been reported as dye sensitizers for DSSC applications. Traditional Ru(II)-based coordination compounds bearing polypyridine ligands commonly contain anionic thiocyanate ligands which can be easily replaced by other ligands into the electrolyte solution, thus reducing the efficiency of the DSSC device. So, there is a growing interest in developing thiocyanate-free Ru(II) dyes. The LUMO levels of **112** and **113** are -2.78 and -3.43 eV, respectively, which suggest a favorable energy level alignment of the dye **112** with the TiO_2 conduction band edge for electron injection but not for **113** [95]. As a result, dye **113** afforded a very poor DSSC performance with PCE of 0.3% only while a higher PCE of 1.5% can be obtained for **112**. Olivier and co-workers then reported another asymmetric Ru-dialkynyl compound **114** with an electron-donating carbazole unit and an anchoring carboxylic acid function [96]. The resulting DSSC is highly efficient in converting sunlight into electrical energy with a broad IPCE profile and a PCE of 7.3%. This represents the best efficiency to date for Ru-acetylide dyes in DSSC utilization and metal-alkynyl complexes in organic solar cells.

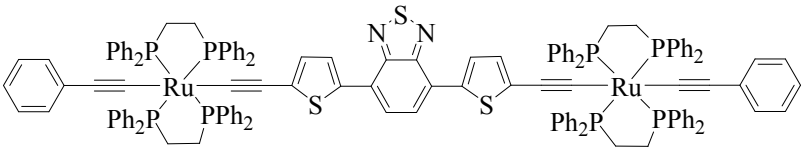

107

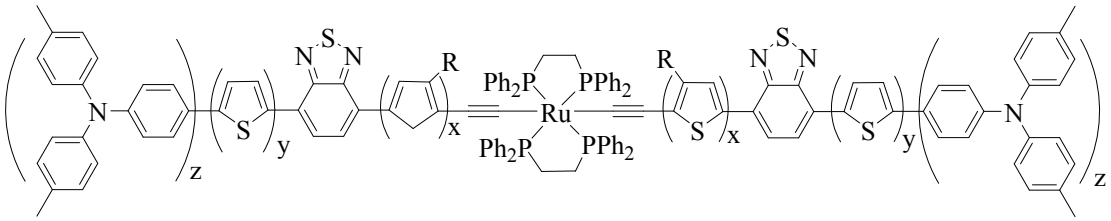

x = 1 (R = H), y = 1, z = 0 **108**
x = 1 (R = C_6H_{13}), y = 0, z = 1 **109**
x = 0, y = 1, z = 1 **110**
x = 1 (R = C_6H_{13}), y = 1, z = 1 **111**

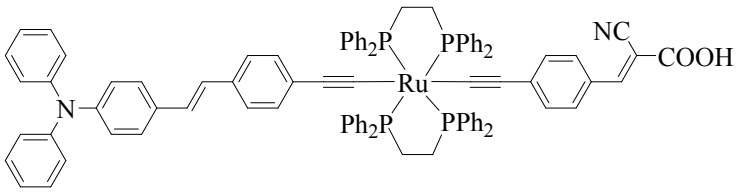

112

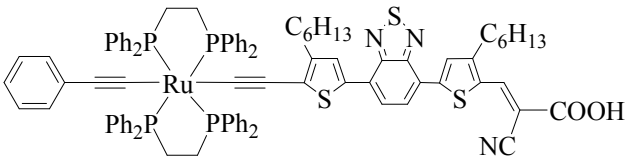

113

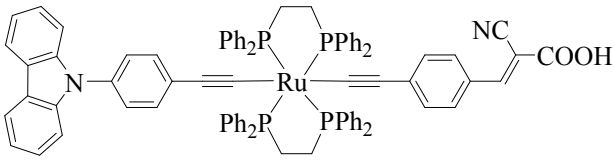

114

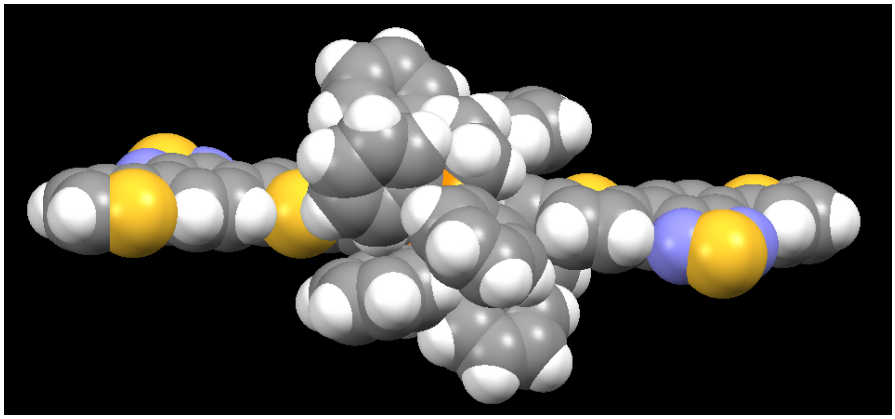

Fig. 13. Space-filling model of **108**.

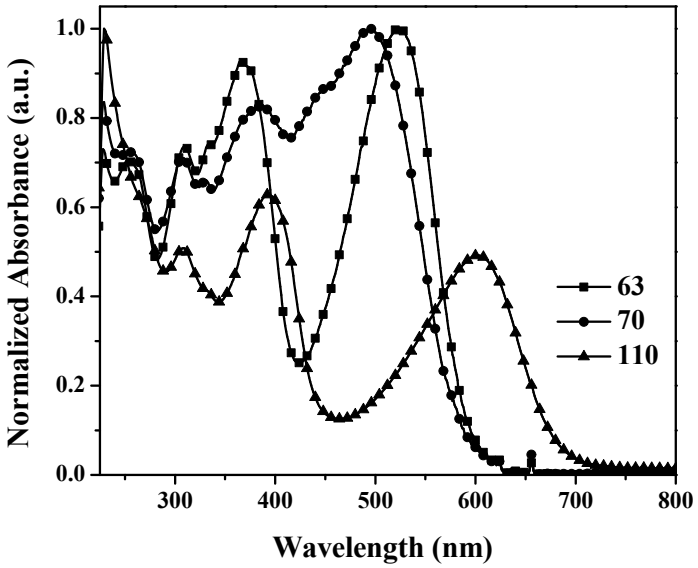

Fig. 14. Absorption spectra of **63**, **70** and **110**.

Table 5

Summary of frontier energy levels and photovoltaic properties of Ru(II) acetylide complexes.

Molecule	Optical bandgap [eV]	HOMO/LUMO [eV]	V_{oc} [V]	J_{sc} [mA cm^{-2}]	FF	PCE [%]	Ref.
107	1.66	−4.74/−3.07	0.40	0.66	0.31	0.10	[93]
108	1.83	−5.21/−3.68	0.51	4.24	0.31	0.66	[94]
109	1.79	−5.27/−3.59	0.41	1.54	0.22	0.14	[94]
110	1.80	−5.23/−3.64	0.40	1.11	0.22	0.14	[94]
111	1.70	−5.12/−3.61	0.46	2.27	0.25	0.25	[94]
112	-	-/−2.78	0.58	4.60	0.56	1.50	[95]
113	-	-/−3.43	0.43	1.50	0.47	0.30	[95]
114	2.10	−4.83/−2.73	0.68	15.56	0.692	7.32	[96]

5. Concluding remarks and future perspectives

The bulk of global energy supply is derived from fossil fuel that is unsustainable and poses considerable threat to our environment. Given the vital role of energy in our society, policymakers, scientists, and technologists are working together to find alternatives that are sustainable and clean. Photovoltaic devices are able to convert (sun)light directly into electrical energy without any emissions of air pollutants and greenhouse gases. Much research has gone into producing efficient organic solar cells. Although inorganic materials have so far dominated the field, organic materials as photovoltaics are also attracting a lot of research attention because of their favorable environmental and inexpensive features. Materials scientists are exploring the rich chemistry of the transition metals to develop new energy technologies and incorporating transition metals into conjugated organic materials is a proven strategy to afford new functional materials and is a vibrant research field in materials science. The redox activity, optical and electronic properties of these metals offer many opportunities to efficiently transport electrons or energy. For instance, transition metals are conjugated into polymers to harvest sunlight, transport excitons, and promote charge separation and transfer in photovoltaic cells. The absorption properties of the metal-organic materials can be manipulated by a careful selection of the organic spacers (Fig. 15). Although most of these developments are still far from

commercialization, the results are impactful. To push the frontiers forward, we need more understanding of the chemistry of the transition metals, especially their redox, optical, and electronic properties in the excited state [97−101]. Such fundamental understanding will be helpful in harvesting sunlight and transporting photo-generated charges to enhance the efficiency of photovoltaic cells.

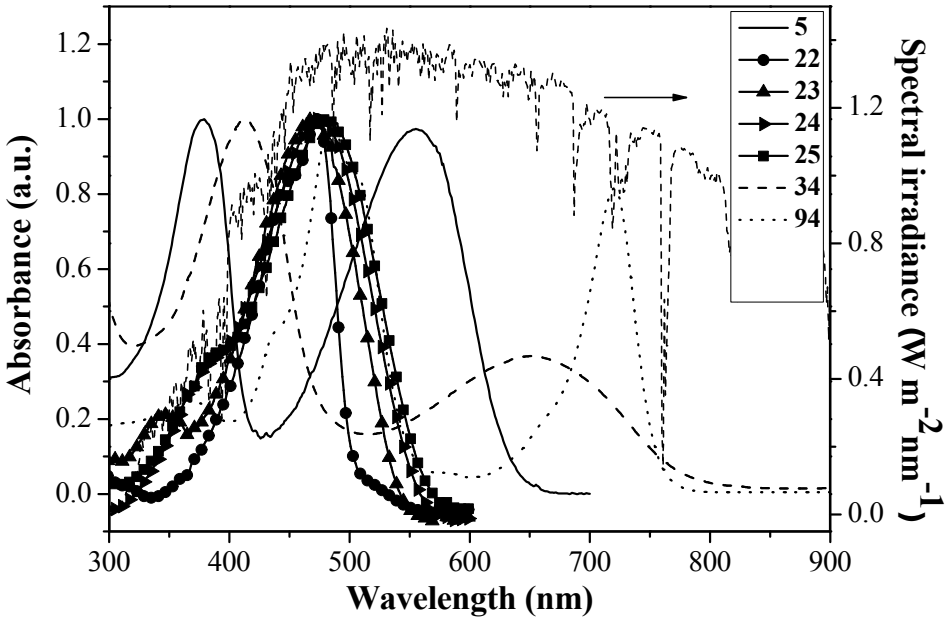

Fig. 15. Absorption spectra of some polyplatinaynes and metalloporphyrins showing a wide absorption range as compared to the standard AM 1.5 solar spectrum.

There is a growing interest in using metal-based donor materials in advancing the PSC/OSC field. Apart from Pt-polyyne donor materials in PSCs, the mercury(II) polyyne polymer **115** with amino-functionalized side chains was recently reported to be a good cathode interlayer of inverted PSCs with the configuration of

ITO/**115**/**PTB7**:$PC_{71}BM$/MoO_3/Al by improving the electron transport and collection properties [102]. Using this interlayer, the device performance was much improved from 3.18 to 9.11%. The authors attributed the PCE enhancement to the importance of the presence of intermolecular interactions for the polymer chains of **115**, such as the Hg···Hg interaction and π-π stacking, which can promote charge transport. The potent electron-transporting features of **115** were demonstrated in the electron-only devices. For comparison, the inverted PSC using **115a** without the amino termini only furnished a moderate PCE of 5.98% since **115a** cannot effectively reduce the work function of the ITO substrate. Huang et al. reported that triplet iridium(III) complex can be incorporated at very low concentration ratios (0, 0.5, 1, 1.5, 2.5 and 5 mol%) into the polymer backbone of **PTB7** through coordination of Ir with dibenzoylmethane auxiliary ligand linkage to give metallopolymer **116** [103]. By increasing the ratio of Ir complexes from 0 to 2.5%, the PCE of the solar cell based on **116** was dramatically enhanced due to the participation of triplet effects. Further increase of the concentration of triplet heavy metal complex to 5% dropped the PCE. The PSC based on **116** at 1% of Ir complex gave an average PCE of 8.04% with V_{oc} = 0.75 V, J_{sc} = 16.0 mA cm^{-2} and FF = 0.67 (versus **PTB7** at PCE = 5.80%, V_{oc} = 0.75 V, J_{sc} = 12.88 mA cm^{-2} and FF = 0.60). From these results, apart from developing totally new materials, introduction of triplet content to existing high-efficiency

photovoltaic organic polymers can also offer a promising avenue to break through the PCE of BHJ PSCs. Very recently, the same research team introduced a heavy platinum(II) complex at various low ratios (0, 1, 1.5 and 5 mol%) as the third monomer for polymerization through a cyclometalated main ligand to make metallopolymer **117** using a random terpolymer molecular design [104]. The polymer containing 1.5 mol% Pt furnished an improved PCE of 8.45% relative to that of the control copolymer (7.92%) even with a much lower molecular weight. The enhancement in PCE was attributed to the higher hole mobility, less bimolecular recombination and more efficient slow charge separation process. High-performance OSCs comprising gold(III) corroles **118**−**120** as electron donor materials in combination with C_{70} as the acceptor have also been fabricated by vacuum evaporation [105]. These heavy-metal small molecules possess long-lived excited state (lifetime ≥ 25 ms) and low emission quantum yield (< 0.15%). They afforded vacuum-evaporated OSCs with PCEs ranging from 1.8 to 3.0% and the PCE can be further elevated to 4% by post thermal annealing for the device based on the **119** (5%):C_{70} active layer. A solution-processed solar cell based on **119**:**PTB7**:$PC_{71}BM$ can even be realized. Two supramolecular self-assembled Ru(II) polymers bearing cyclopentadithiophene-benzothiadiazole bridges **121**−**122** were also prepared which showed good solubility in organic solvents and excellent thermal stability [106].

These polymers possess low E_g (1.60 eV for **121** and 1.58 eV for **122**) and low-lying HOMO levels (−5.22 eV for **121** and −5.27 eV for **122**). BHJ devices with the structure of ITO/PEDOT:PSS/**121** or **122**:$PC_{71}BM$/Ca/Al furnished decent PCE of 1.99% and 2.66% for **121** and **122**, respectively, even without any additives and/or post-treatment of the active layer films. The fluorine atom effect was clearly demonstrated in this work.

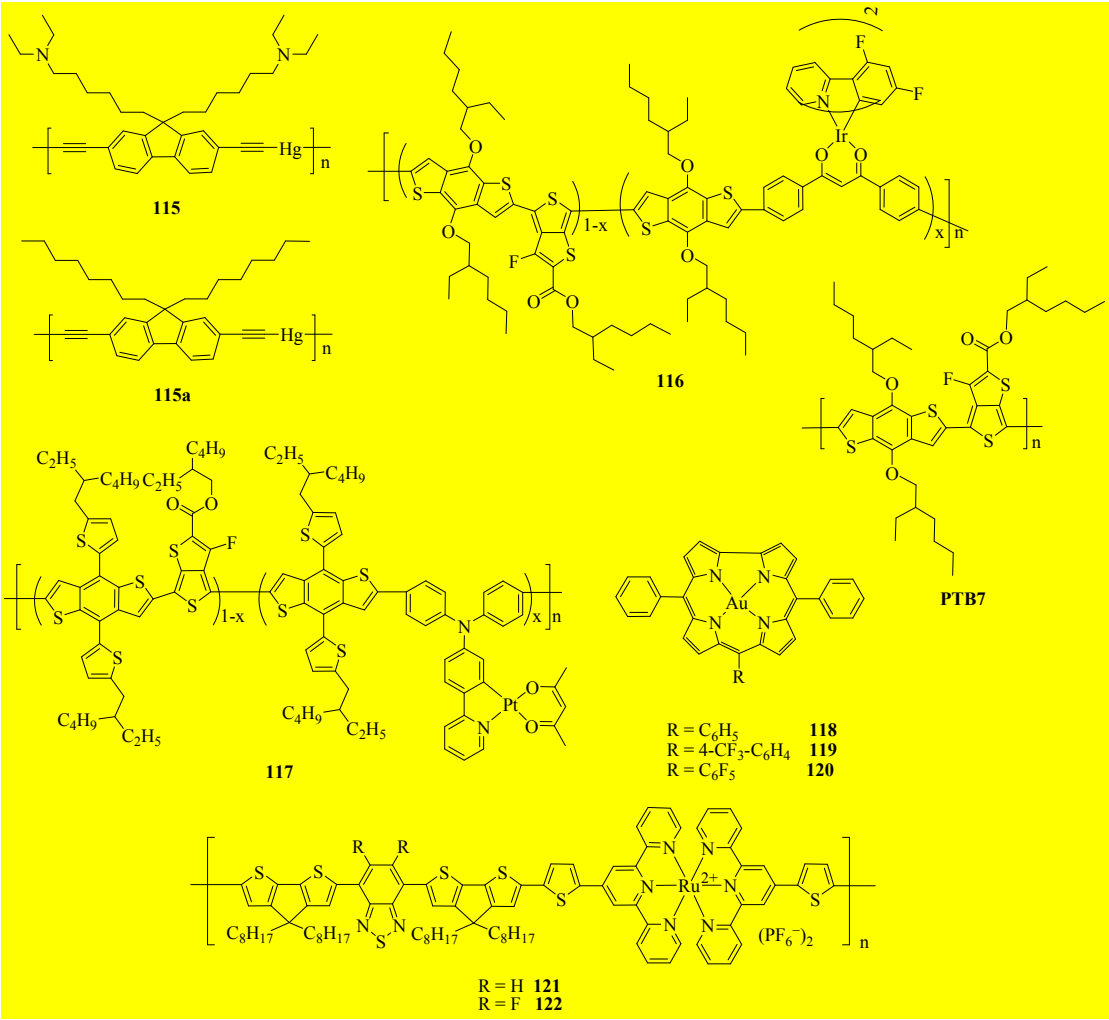

To conclude, metallayne chemistry can and will make important contribution to the global energy problem. A large number of scientists have reported on the different

types of low-bandgap molecular and polymeric metallaynes and related compounds that can function as molecular donors or photosensitizers for organic and dye-sensitized solar cells to convert optical energy to electrical power. These compounds are of paramount importance to achieve a breakthrough in the OSC and DSSC developments. We are looking forward to these developments with much optimism. Therefore, it is worthwhile investigating polymetallaynes and related molecules in the guest for developing new metal-based donor materials for OSC applications. A better understanding and an appreciation of these metalated dyes can serve as a significant asset for researchers to develop next generation efficient solar cell materials. These metal-based functional molecules offer many exciting future challenges for both exploratory and applications-oriented research. Clearly, the cost of materials and device durability are issues that need to be addressed in the future development and commercialization.

Acknowledgements

We are grateful to the financial support from Hong Kong Research Grants Council of HKSAR (HKBU 203313), Areas of Excellence Scheme, University Grants Committee of HKSAR (AoE/P-03/08), the National Natural Science Foundation of China (project number 21671061), and the Hong Kong Polytechnic University (1-

ZE1C).

References

1. International Energy Agency, World Energy Outlook 2016: Executive Summary, International Energy Agency, Paris, France (2016).
2. D. Gielen, F. Boshell, D. Saygin, Nat. Mater. 15 (2016) 117−120.
3. United States Energy Information Administration, International Energy Outlook 2016, US Energy Information Administration, Washington DC, USA (2016).
4. J.A. Turner, Science 285 (1999) 687−689.
5. R. Eisenberg, D.G. Nocera, Inorg. Chem. 44 (2005) 6799−6801.
6. A. Bosio, N. Romeo, A. Podesta, S. Mazzamuto, V. Canevari, Cryst. Res. Technol. 40 (2005) 1048−1053.
7. M.T. Lloyd, J.E. Anthony, G.G. Malliaras, Mater. Today 10 (2007) 34−41.
8. S. Günes, H. Neugebauer, N.S. Sariciftci, Chem. Rev. 107 (2007) 1324−1338.
9. B.C. Thompson, J.M. Frechet, Angew. Chem. Int. Ed. 47 (2008) 58−77.
10. Y.-J. Cheng, S.-H. Yang, C.-S. Hsu, Chem. Rev. 109 (2009) 5868−5923.
11. G. Dennler, M.C. Scharber, C.J. Brabec, Adv. Mater. 21 (2009) 1323−1338.
12. M. Pagliaro, R. Ciriminna, G. Palmisano, ChemSusChem 1 (2008) 880−891.
13. G. Yu, J. Gao, J.C. Hummelen, F. Wudl, A.J. Heeger, Science 270 (1995) 1789−1791.

14. W.-Y. Wong, C.-L. Ho, Acc. Chem. Res. 43 (2010) 1246−1256.

15. M. Pope, C.E. Swenberg, Electronic Processes in Organic Crystals and Polymers; Oxford University Press: Oxford, U.K. (1999).

16. G. Li, V. Shrotriya, Y. Yao, J. Huang, Y. Yang, J. Mater. Chem. 17 (2007) 3126−3140.

17. P. Heremans, D. Cheyns, B.P. Rand, Acc. Chem. Res. 42 (2009) 1740−1747.

18. Y. Liu, S. Wang, Y. Tao, W. Huang, Chin. Chem. Lett. 27 (2016) 1250−1258.

19. S. Goswami, M.K. Gish, J. Wang, R.W. Winkel, J.M. Papanikolas, K.S. Schanze, ACS Appl. Mater. Interfaces 7 (2015) 26828−26838.

20. J. Mei, K. Ogawa, Y. Kim, N.C. Heston, D.J. Arenas, Z. Nasrollahi, T.D. McCarley, D.B. Tanner, J.R. Reynolds, K.S. Schanze, ACS Appl. Mater. Interfaces 1 (2009) 150−161.

21. F. Guo, Y. Kim, J.R. Reynolds, K.S. Schanze, Chem. Commun. 17 (2006) 1887−1889.

22. F. Guo, K. Ogawa, Y. Kim, E.O. Danilov, F.N. Castellano, J.R. Reynolds, K.S. Schanze, Phys. Chem. Chem. Phys. 9 (2007) 2724−2734.

23. G.L. Schulz, S. Holdcroft, Chem. Mater. 20 (2008) 5351−5355.

24. J. Peet, M.L. Senatore, A.J. Heeger, G.C. Bazan, Adv. Mater. 21 (2009) 1521−1527.

25. A. Gadisa, M. Svensson, M.R. Andersson, O. Inganas, Appl. Phys. Lett. 84 (2004) 1609−1611.

26. M.C. Scharber, D. Mühlbacher, M. Koppe, P. Denk, C. Waldauf, A.J. Heeger, C.J. Brabec, Adv. Mater. 18 (2006) 789−794.

27. J.-L. Brédas, D. Beljonne, V. Coropceanu, J. Cornil, Chem. Rev. 104 (2004) 4971−5003.

28. U.H.E. Bunz, Chem. Rev. 100 (2000) 1605−1644.

29. W.-Y. Wong, Dalton Trans. 40 (2007) 4495−4510.

30. C.-L. Ho, Z.-Q Yu, W.-Y. Wong, Chem. Soc. Rev. 45 (2016) 5264−5295.

31. L. Schull, J.G. Kushmerick, C.H. Patterson, C. George, M.H. Moore, S.K. Pollack, R. Shashidhar, J. Am. Chem. Soc. 125 (2003) 3202−3203.

32. G. Frapper, M. Kertesz, Inorg. Chem. 32 (1993) 732−740.

33. A. Köhler, H.F. Wittmann, R.H. Friend, M.S. Khan, J. Lewis, Synth. Met. 67 (1994) 245−249.

34. A. Köhler, H.F. Wittmann, R.H. Friend, M.S. Khan, J. Lewis, Synth. Met. 77 (1996) 147−150.

35. N. Chawdhury, A. Köhler, R.H. Friend, W.-Y. Wong, J. Lewis, M. Younus, P.R. Raithby, T.C. Corcoran, M.R.A. Al-Mandhary, M.S. Khan, J. Chem. Phys. 110 (1999) 4963−4970.

36. N. Chawdhury, M. Younus, P.R. Raithby, J. Lewis, R.H. Friend, Opt. Mater. 9 (1998) 498−501.

37. W.-Y. Wong, X.-Z. Wang, Z. He, A.B. Djurišić, C.-T. Yip, K.-Y. Cheung, H. Wang, C.S.K. Mak, W.-K. Chan, Nat. Mater. 6 (2007) 521−527.

38. W.-Y. Wong, C.-L. Ho, Coord. Chem. Rev. 250 (2006) 2627−2690.

39. M. Lenes, L.J.A. Koster, Appl. Phys. Lett. 88 (2006) 243502−243505.

40. W.-Y. Wong, X.Z. Wang, H.-L. Zhang, K.-Y. Cheung, M.-K. Fung, A.B. Djurišić, W.-K. Chan, J. Organomet. Chem. 693 (2008) 3603−3612.

41. N.S. Baek, S.K. Hau, H.-L, Yip, O. Acton, K.-S. Chen, A.K.-Y. Jen, Chem. Mater. 20 (2008) 5734−5736.

42. Q.W. Wang, W.-Y. Wong, Polym. Chem. 2 (2011) 432−440.

43. P.-T. Wu, T. Bull, F.S. Kim, C.K. Luscombe, S.A. Jenekhe, Macromolecules 42 (2009) 671−681.

44. X.-Z. Wang, C.-L. Ho, L. Yan, X. Chen, X. Chen, K.-Y. Cheung, W.-Y. Wong, J. Inorg. Organomet. Polym. Mater. 20 (2010) 478−487.

45. C.J. Qin, Y.Y. Fu, C.-H. Chui, C.-W. Kan, Z.Y. Xie, L.X. Wang, W.-Y. Wong, Macromol. Rapid Commun. 32 (2011) 1472−1477.

46. Q. Liu, C.-L. Ho, Y.H. Lo, H. Li, W.-Y. Wong, J. Inorg. Organomet. Polym. Mater. 25 (2015) 159−168.

47. W.-Y. Wong, X.-Z. Wang, Z. He, K.-K. Chan, A.B. Djurišić, K.-Y. Cheung, C.-T. Yip, A.M-C. Ng, Y.Y. Xi, C.S.K. Mak, W.-K. Chan, J. Am. Chem. Soc. 129 (2007) 14372–14380.

48. B.L. Liu, C.-L. Ho, W.-Y. Wong, K.-Y. Cheung, M.-K. Fung, W.-T. Lam, A.B. Djurišić, W.-K. Chan, Adv. Funct. Mater. 18 (2008) 2824–2833.

49. W.-Y. Wong, W.-C. Chow, K.-Y. Cheung, M.-K. Fung, A.B. Djurišić, W.-K. Chan, J. Organomet. Polym. 694 (2009) 2717–2726.

50. X.-Z. Wang, Q. Wang, L. Yan, W.-Y. Wong, K.-Y. Cheung, A. Ng, A.B. Djurišić, W.-K. Chan, Macromol. Rapid Commun. 31 (2010) 861–867.

51. H.M. Zhan, W.-Y. Wong, A. Ng, A.B. Djurišić, W.-K. Chan, J. Organomet. Polym. 696 (2011) 4112–4120.

52. L. Li, W.-C. Chow, W.-Y. Wong, C.-H. Chui, R. S.-M. Wong, J. Organomet. Polym. 696 (2011) 1189–1197.

53. Q.W. Wang, Z. He, A. Wild, H.B. Wu, Y. Cao, U.S. Schubert, C.-H. Chui, W.-Y. Wong, Chem. Asian J. 6 (2011) 1766–1777.

54. K. Sonogashira, H. Morimoto, Y. Takai, S. Takahashi, Symp. Organomet. Chem. Jpn. 28 (1981) 64–66.

55. Y. Yuan, T. Michinobu, Macromol. Chem. Phys. 213 (2012) 2114–2119.

56. Yuan, T. Michinobu, J. Oguma, T. Kato, K. Miyake, Macromol. Chem. Phys. 214

(2013) 1465–1472.

57. T. Michinobu, All-Polymer Solar Cells based on Organometallics Polymers. Chapter 5, 115–135 in "Organometallics and Related Molecules for Energy Conversion" (Ed. W.-Y. Wong) 2015.

58. X. Zhao, C. Poliego, B. Kim, D.A. Poulsen, B. Ma, D.A. Unruh, J.M. Fréchet, Chem. Mater. 22 (2010) 2325–2332.

59. C.H. Cui, Y.Y. Zhang, W.C.H. Choy, H. Li, W.-Y. Wong, Sci. China Chem. 58 (2015) 347–356.

60. F.-R. Dai, H.-M. Zhan, Q. Liu, Y.-Y. Fu, J.-H. Li, Q.-W. Wang, Z.Y. Xie, L.X. Wang, F. Yan, W.-Y. Wong, Chem. Eur. J. 18 (2012) 1502–1511.

61. W.H. He, M.Y. Livshits, D.A. Dickie, J.Z. Yang, R. Quinnett, J.J. Rack, Q. Wu, Y. Qin, Chem. Sci. 7 (2016) 5798–5804.

62. W.H. He, M.Y. Livshits, D.A. Dickie, Z. Zhang, L.E. Mejiaortega, J.J. Rack, Q. Wu, Y. Qin, J. Am. Chem. Soc. 139 (2017) 14109–14119.

63. P.G. Bomben, K.C.D. Robson, B.D. Koivisto, C.P. Berlinguette, Coord. Chem. Rev. 256 (2012) 1438–1450.

64. C.E. Houseroft, E.C. Constable, Chem. Soc. Rev. 44 (2015) 8386–8398.

65. C.-L. Ho, W.-Y. Yang, J. Photochem. Photobio. C: Photochem. Rev. 28 (2016) 138–158.

66. A. Hagfeldt, G. Boschloo, L. Sun, L. Kloo, H. Pettersson, Chem. Rev. 110 (2010) 6595−6663.

67. S. Zhang, X. Yang, Y. Numatta, L. Han, Energy Environ. Sci. 6 (2013) 1443−1464.

68. W.-K. Chan, C.S. Hui, K.Y.K. Man, K.W. Cheng, H.L. Wong, G. Viscardi, P. Liska, S. Ito, T. Bessho, M. Grätzel, J. Am. Chem. Soc. 127 (2005) 16835−16847.

69. A. Altobello, R. Argazzi, S. Caramori, C. Contado, S. Da Fré, P. Rubino, C. Choné, G. Larramona, C.A. Bignozzi, J. Am. Chem. Soc. 127 (2005) 15342−15343.

70. E.I. Mayo, K. Kilsa, T. Tirrell, P.I. Djurovich, A. Tamayo, M.E. Thompson, N.S. Lewis, H.B. Gray, Photochem. Photobio. Sci. 5 (2006) 871−873.

71. F.-R. Dai, Y.-C. Chen, L.-F. Lai, W.-J. Wu, C.-H. Cui, G.-P. Tan, X.-Z. Wang, J.-T. Lin, H. Tian, W.-Y. Wong, Chem. Asian J. 7 (2012) 1426−1434.

72. W.J. Wu, X.D. Xu, H.B. Yang, J.L. Hua, X.Y. Zhang, L. Zhang, Y.T. Long, H. Tian, J. Mater. Chem. 21 (2011) 10666−10671.

73. C.-H. Siu, L.T.L. Lee, S.-C. Yiu, P.-Y. Ho, P.W. Zhou, C.-L. Ho, T. Chen, J.Y. Liu, K.L. Han, W.-Y. Wong, Chem. Eur. J. 22 (2016) 3750−3757.

74. F.Q. Guo, K. Ogawa, Y.-G. Kim, E.O. Danilov, F.N. Castellano, J.R. Reynolds, K.S. Schanze, Phys. Chem. Chem. Phys. 9 (2007) 2724−2734.

75. X.B. Huang, C.L. Zhu, S.M. Zhang, W.W. Li, Y.L. Guo, X.W. Zhan, Y.Q. Liu, Z.S. Bo, Macromolecules 41 (2008) 6895−6902.

76. X.G. Zhao, L.C. Ma, L. Zhang, Y.G. Wen, J.M. Chen, Z.G. Shuai, Y.Q. Liu, X.W. Zhan, Macromolecules 46 (2013) 2152−2158.

77. H.M. Zhan, S. Lamare, A. Ng, T. Kenny, H. Guernon, W.-K. Chan, A.B. Djurišić, P.D. Harvey, W.-Y. Wong, Macromolecules 44 (2011) 5155−5167.

78. Y.-H. Chao, J.-F. Jheng, J.-S. Wu, K.-Y. Wu, H.-H. Peng, M.-C. Tsai, C.L. Wang, Y.-N. Hisao, C.-L. Wang, C.-Y. Lin, C.-S. Hsu, Adv. Mater. 26 (2014) 5205−5210.

79. C.V. Kumar, L. Cabau, E.N. Koukaras, G.D. Sharma, E. Palomares, Nanoscale 7 (2015) 179−189.

80. Y.Y. Huang, L.S. Li, X.P. Peng, J.B. Peng, Y. Cao, J. Mater. Chem. 22 (2012) 21841−21844.

81. L.S. Li, Y.Y. Huang, J.B. Peng, Y. Cao, X.B. Peng, J. Mater. Chem. A 1 (2013) 2144−2150.

82. H.M. Qin, L.S. Li, F.Q. Guo, S.J. Su, J.B. Peng, Y. Cao, X.B. Peng, Energy Environ. Sci. 7 (2014) 1397−1401.

83. K. Gao, J.S. Miao, L.G. Xiao, W.Y. Deng, Y.Y. Kan, T.X. Liang, C. Wang, F. Huang, J.B. Peng, Y. Cao, F. Liu, T.P. Russell, H.B. Wu, X.B. Peng, Adv. Mater.

28 (2016) 4727–4733.

84. M.M. Li, K. Gao, X.J. Wan, Q. Zhang, B. Kan, R.X. Xia, F. Liu, X. Yang, H.R. Feng, W. Ni, Y.C. Wang, J.J. Peng, H.T. Zhang, Z.Q. Liang, H.-L. Yip, X.B. Peng, Y. Cao, Y.S. Chen, Nat. Photon. 11 (2017) 85–90.

85. S. Chen, L.G. Xiao, X.J. Zhu, X.B. Peng, W.-K. Wong, W.-Y. Wong, Chem. Commun. 51 (2015) 14439–14442.

86. H.D. Wang, L.G. Xiao, L. Yan, S. Chen, X.J. Zhu, X.B. Peng, X.Z. Wang, W.-K. Wong, W.-Y. Wong, Chem. Sci. 7 (2016) 4301–4307.

87. L.G. Xiao, S. Chen, K. Gao, X.B. Peng, F. Liu, Y. Cao, W.-Y. Wong, W.-K. Wong, X.J. Zhu, ACS Appl. Mater. Interfaces 8 (2016) 30176–30183.

88. J.F. Lu, B.Y. Zhang, H.L. Yuan, X.B. Xu, K. Cao, J. Cui, S.S. Liu, Y. Shen, Y.B. Cheng, J. Xu, M.K. Wang, J. Phys. Chem. C 118 (2014) 14739–14748.

89. T. Bessho, S.M. Zakeeruddin, C.-Y. Yeh, E.W-.G. Diau, M. Grätzel, Angew. Chem. Int. Ed. 49 (2010) 6646–6649.

90. A. Yella, H.-W. Lee, H.N. Tsao, C.Y. Yi, A.K. Chandiran, M.K. Nazeeruddin, E.W.-G. Diau, C.-Y. Yeh, S.M. Zakeeruddin, M. Grätzel, Science 334 (2011) 629–634.

91. A. Yella, C.-L. Mai, S.M. Zakeeruddin, S.-N. Chang, C.-H. Hsieh, C.-Y. Yeh, M. Grätzel, Angew. Chem. Int. Ed. 53 (2014) 2973–2977

92. S. Mathew, A. Yella, P. Gao, R. Humphty-Baker, B.F.E. Curchod, N. Ashari-Astani, L. Tavernelli, U. Rothlisberger, M.K. Nazeeruddin, M. Grätzel, Nat. Chem. 6 (2014) 242–247.

93. A. Colombo, C. Dragonetti, D. Roberto, R. Ugo, L. Falciola, S. Luzzati, D. Kotowski, Organometallics 30 (2011) 1279–1282.

94. Q. Liu, C.-L. Ho, N.Y. Zhu, Y.Y. Fu, Z.Y. Xie, L.X. Wang, P.D. Harvey, W.-Y. Wong, J. Organomet. Chem. 846 (2017) 277–286.

95. F. Nisic, A. Colombo, C. Dragonetti, E. Garoni, D. Marinotto, S. Righetto, F.D. Angelis, M.G. Lobello, P. Salvatori, P. Biagini, F. Melchiorre, Organometallics 34 (2015) 94–104.

96. S.D. Sousa, L. Ducasse, B. Kauffmann, T. Toupance, C. Olivier, Chem. Eur. J. 20 (2014) 7017–7024.

97. H. Xu, R.F. Chen, Q. Sun, W.Y. Lai, Q.Q. Su, W. Huang, X.G. Liu, Chem. Soc. Rev. 43 (2014) 3259–3302.

98. J. Xiang, C.-L. Ho, W.-Y. Wong, Polym. Chem. 6 (2015) 6905–6930.

99. G.R. Whittell, M.D. Hager, U.S. Schubert, I. Manners, Nat. Mater. 10 (2011) 176–188.

100. S.-J. Liu, Y. Chen. W.-J. Xu, Q. Zhao, W. Huang, Macromol. Rapid Commun. 33 (2012) 461–480.

101. A.S. Abd-El-Aziz, E.A. Strohm, Polymer 53 (2012) 4879–4921.

102. S.J. Liu, K. Zhang, J.M. Lu, J. Zhang, H.-L. Yip, F. Huang, Y. Cao, J. Am. Chem. Soc. 135 (2013) 15326–15329.

103. M. Qian, R. Zhang, J.Y. Hao, W.J. Zhang, Q. Zhang, J.P. Wang, Y.T. Tao, S.F. Chen, J.F. Fang, W. Huang, Adv. Mater. 27 (2015) 3546–3552.

104. Z. Wan, J. Yang, Y.N. Liu, S.F. Wang, Y. Zhong, C. Li, Z.G. Zhang, G.C. Xing, S. Huettner, Y.T. Tao, Y.F. Li, W. Huang, Polym. Chem. 8 (2017) 4729–4737.

105. S.-L Lai, L. Wang, C. Yang, M.-Y. Chan, X.G. Guan, C.-C. Kwok, C.-M. Che, Adv. Funct. Mater. 24 (2014) 4655–4665.

106. K. Feng, X. Shen, Y. Li, Y. He, D. Huang, Q. Peng, Polym. Chem. 4 (2013) 5701−5710.